minerals

MDPI

Article

Dissimilatory Iron-Reducing Microorganisms Are Present and Active in the Sediments of the Doce River and Tributaries Impacted by Iron Mine Tailings from the Collapsed Fundão Dam (Mariana, MG, Brazil)

Carolina N. Keim [1,*], Jilder D. P. Serna [2], Daniel Acosta-Avalos [2], Reiner Neumann [3], Alex S. Silva [1,4], Diogo A. Jurelevicius [1], Raphael S. Pereira [1], Pamella M. de Souza [1], Lucy Seldin [1] and Marcos Farina [5]

[1] Instituto de Microbiologia Paulo de Góes, Universidade Federal do Rio de Janeiro—UFRJ, Av. Carlos Chagas Filho, 373, Cidade Universitária, Rio de Janeiro 21941-902, RJ, Brazil; alexss2502@gmail.com (A.S.S.); diogoj@micro.ufrj.br (D.A.J.); raphael.pereira@ufrj.br (R.S.P.); pamella@eq.ufrj.br (P.M.d.S.); lseldin@micro.ufrj.br (L.S.)

[2] Centro Brasileiro de Pesquisas Físicas—CBPF, Av. Xavier Sigaud 150, Urca, Rio de Janeiro 22290-180, RJ, Brazil; jilderpea@gmail.com (J.D.P.S.); dacosta@cbpf.br (D.A.-A.)

[3] Centro de Tecnologia Mineral—CETEM, Av. Pedro Calmon 900, Cidade Universitária, Rio de Janeiro 21941-908, RJ, Brazil; rneumann@cetem.gov.br

[4] Departamento de Microbiologia, Imunologia e Parasitologia, Universidade Federal de São Paulo–UNIFESP, São Paulo 04023-062, SP, Brazil

[5] Instituto de Ciências Biomédicas, Universidade Federal do Rio de Janeiro–UFRJ, Av. Carlos Chagas Filho, 373, Cidade Universitária, Rio de Janeiro 21941-902, RJ, Brazil; mfarina@icb.ufrj.br

* Correspondence: cnkeim@micro.ufrj.br

Citation: Keim, C.N.; Serna, J.D.P.; Acosta-Avalos, D.; Neumann, R.; Silva, A.S.; Jurelevicius, D.A.; Pereira, R.S.; de Souza, P.M.; Seldin, L.; Farina, M. Dissimilatory Iron-Reducing Microorganisms Are Present and Active in the Sediments of the Doce River and Tributaries Impacted by Iron Mine Tailings from the Collapsed Fundão Dam (Mariana, MG, Brazil). *Minerals* **2021**, *11*, 244. https://doi.org/10.3390/min11030244

Academic Editor: Juan Antelo

Received: 3 January 2021
Accepted: 22 February 2021
Published: 26 February 2021

Abstract: On 5 November 2015, a large tailing deposit failed in Brazil, releasing an estimated 32.6 to 62 million m^3 of iron mining tailings into the environment. Tailings from the Fundão Dam flowed down through the Gualaxo do Norte and Carmo riverbeds and floodplains and reached the Doce River. Since then, bottom sediments have become enriched in Fe(III) oxyhydroxides. Dissimilatory iron-reducing microorganisms (DIRMs) are anaerobes able to couple organic matter oxidation to Fe(III) reduction, producing CO_2 and Fe(II), which can precipitate as magnetite ($FeO{\cdot}Fe_2O_3$) and other Fe(II) minerals. In this work, we investigated the presence of DIRMs in affected and non-affected bottom sediments of the Gualaxo do Norte and Doce Rivers. The increase in Fe(II) concentrations in culture media over time indicated the presence of Fe(III)-reducing microorganisms in all sediments tested, which could reduce Fe(III) from both tailings and amorphous ferric oxyhydroxide. Half of our enrichment cultures converted amorphous Fe(III) oxyhydroxide into magnetite, which was characterized by X-ray diffraction, transmission electron microscopy, and magnetic measurements. The conversion of solid Fe(III) phases to soluble Fe(II) and/or magnetite is characteristic of DIRM cultures. The presence of DIRMs in the sediments of the Doce River and tributaries points to the possibility of reductive dissolution of goethite (α-FeOOH) and/or hematite (α-Fe_2O_3) from sediments, along with the consumption of organics, release of trace elements, and impairment of water quality.

Keywords: Rio Doce; Gualaxo do Norte; Mariana; Fundão Dam; tailings; bottom sediments; dissimilatory iron-reducing bacteria; goethite; hematite; magnetite

1. Introduction

Dissimilatory iron-reducing microorganisms (DIRMs) couple the oxidation of organics to iron reduction, generating a proton-motive force used for many energy-requiring activities, including ATP synthesis and growth [1–4]. They are widespread in anaerobic sediments and have been affiliated with several distinct bacterial and archaeal phyla. Currently, the most studied species belong to the bacterial genera *Geobacter* and *Shewanella* [5].

Enrichment cultures of DIRMs have been obtained from diverse anaerobic environments, mainly sediments and soils [6–15]. In defined media, organic electron donors for Fe(III) reduction are usually acetate [6–8,10–13,15] and/or lactate [15,16]. Fe(III) sources include either soluble, chelated Fe(III) [8,11,12] or synthetic, amorphous or poorly crystalline Fe(III) oxyhydroxides [6–8,10,13,15]. Synthetic crystalline iron oxides, such as 6-line ferrihydrite, lepidocrocite (γ-FeOOH), goethite (α-FeOOH), hematite (α-Fe_2O_3), magnetite ($FeO{\cdot}Fe_2O_3$), scorodite ($FeAsO_4{\cdot}2H_2O$), and jarosite, and other minerals from the alunite group (e.g., $KFe_3(OH)_6(SO_4)_2$, $NH_4Fe_3(OH)_6(SO_4)_2$, $AgFe_3(OH)_6(SO_4)_2$, and arsenic-doped schwertmannite ($Fe_{16}O_{16}(OH)_{9.6}$ $(SO_4)_{3.2}O_{16}{\cdot}10H_2O$)) have been used as Fe(III) sources for DIRMs in vitro [17–27]. Natural Fe(III)-containing materials reduced by *Shewanella* species include goethite and hematite from subsurface sediments [19], goethite from iron ore [28], poorly crystalline ferrihydrite and lepidocrocite from a freshwater biofilm [29], soil [18], lake sediments [20,30], and uranium mill tailings [31]. Similarly, enrichment cultures were able to use natural materials as Fe(III) sources, including both amorphous [8] and crystalline Fe(III) oxides [16].

Several dissimilatory iron-reducing bacterial cultures produce mixed-valence iron oxide magnetite [8,13,18,23,24,26,29,32–42]. Other crystalline products of Fe(III) reduction to Fe(II) by DIRMs include vivianite ($Fe_3(PO_4)_{2{\cdot}8}H_2O$) [8,19,29,33,43], siderite ($FeCO_3$) [19,33,35,36,42,43], and green rust ($Fe_6(OH)_{12}CO_3{\cdot}3H_2O$) [20,29,33,43,44]. The production of small amounts of hematite, goethite, lepidocrocite, and/or akaganeite (β-FeOOH) was also reported in pure cultures of DIRMs [26,34,36,40,42,43,45].

The importance of DIRMs in natural environments is multifold, for example, for (i) anaerobic degradation of organic matter, including recalcitrant molecules; (ii) influence on the extent of methane (CH_4) production in freshwater environments; (iii) soil gleying; (iv) steel corrosion; (v) genesis of high dissolved Fe(II) concentrations in aquifers; (vi) magnetite, vivianite, and siderite precipitation in soils and sediments; and (vii) release of phosphate and trace metals bound to iron oxides into water [2,3]. Trace elements released by cultured DIRMs include As [20,45,46], Cd [40], Co [30,47], Cr [30], Mn [30,48], Ni [30,44,47], U [49], Ba, Ra [31], Cu, and Zn [48]. On the other hand, magnetite nanoparticles produced by DIRMs can scavenge metals from the culture medium, including As [22], Cr [36], Mg [38], Mn [13,38], Co, Ni, and Zn [13]. Thus, DIRM activities can lead to both dissolution and precipitation of metal(loid)s in soils and sediments, depending on local conditions.

In November 2015, an iron mining tailing dam owned by Samarco Company collapsed in Brazil, releasing an estimated 32.6 to 62 million m^3 of tailings into the environment [50–53]. Tailings from the Fundão Dam first reached Santarém Stream and then ran downstream into Gualaxo do Norte, Carmo, and Doce Rivers, leading to a large flood. Nineteen people were killed, a nearby village was destroyed, several buildings along the river were damaged, the riparian forest was ripped out, most riverine fish were killed, and crops and pastures were buried under a thick layer of tailings mixed with river sediments. Then, tailings followed the Doce River mainstream, and almost a month later, they reached the Atlantic Ocean, creating a plume of turbidity. The public water supply to approximately 400,000 people was interrupted for a few weeks, as well as industrial activities, electricity generation in three hydroelectric plants, fishing, tourism, and agriculture [52]. Five years later, large amounts of tailings remained in the bottom sediments of the Doce River and its tributaries the Carmo River, the Gualaxo do Norte River, and the Santarém Stream [54–56].

The material deposited by the flood along the banks of the Gualaxo do Norte River consisted of 4.5% coarse sand, 37.5% fine sand, 47.5% silt, and 10.6% clay, with a specific surface area of 5.25 m^2g^{-1} and a TOC (total organic carbon) of 1.51 mg g^{-1} [57]. Bottom sediments from six points downstream of the Fundão Dam showed a predominance of very fine sand, silt/clay, and fine sand, with organic matter below 0.5% [54]. Comparison with tailings, upstream sediments, and data obtained before dam burst indicated that tailings “covered up and/or dragged the old sediments” of the Gualaxo do Norte River [54]. Water pH varied from 6.8 to 7.7, whereas E_H was 82-188, indicating oxidizing conditions in areas highly affected by tailings [54]. The mineral composition of the Fundão Dam tailings was 45–64% quartz (SiO_2), 24–31% hematite, 3.8–16.0% goethite, 1.4–5.1% kaolinite ($Al_2Si_2O_5(OH)_4$), 0.6–1.0% magnetite, and 1.9–2.4% biotite ($K(Fe^{2+}/Mg)_2(Al/Fe^{3+}/Mg)([Si/Al]Si_2O_{10})(OH/F)_2$) [53]. More than 600 km away, the material collected at the Doce River estuary showed mainly quartz, goethite, hematite, and kaolinite. Solid-phase fractionation revealed iron as a major element in this material, mostly in crystalline phases, as expected. Ni, Cu, and Co in the mg/kg range were mainly associated with the iron crystalline phases, whereas g/kg amounts of Mn were found mainly in the exchangeable and soluble fractions, and mg/kg amounts of Cr, Zn, and Pb were associated with the lepidocrocite fraction. Based on these results, Queiroz et al. discussed the potential for microbial iron reduction coupled with trace metal mobilization in estuarine wetland soils affected by iron mine tailings due to anaerobic degradation of high amounts of organic matter [58]. The Doce River watershed was highly impacted by untreated sewage from at least 870,000 people, which increased the organic and nutrient loads in water and sediments and led to frequent cyanobacterial blooms before dam burst [59]. After dam burst, the presence of high levels of thermotolerant coliforms and DO (dissolved oxygen) below 5 mg/L at several points along the river indicates that discharge of large amounts of untreated sewage is still occurring in the watershed [60]. Here, we extend this rationale to the sediments of the entire Doce River as well as affected tributaries, pointing to the risk of extensive dissolution of iron oxides in the river sediments by DIRMs, releasing trace metals and impairing water quality. Thus, the presence and activities of DIRMs in the Doce River and affected tributaries are major issues regarding metal bioavailability and water quality.

In this work, we used crude enrichments to assess the presence and activities of DIRMs in the sediments of the Doce River and its tributary the Gualaxo do Norte River in areas affected or not affected by Fundão Dam tailings. The fingerprint of the microbial community present in the enrichments was obtained by polymerase chain reaction–denaturing gradient gel electrophoresis (PCR-DGGE) of the 16S rRNA gene. Iron-reducing activities were assessed by quantification of Fe(II) in spent culture media and/or by identification of magnetite, which is a common by-product of DIRM activities, in the solid phase.

2. Materials and Methods

Fieldwork was performed on both the Doce River and its most impacted tributary, the Gualaxo do Norte River (Figure 1). To obtain sediments containing living microorganisms for inoculation of crude enrichment cultures, surface sediment samples were collected at two distinct points of the Gualaxo do Norte River, one at the Mariana Municipality (GNR-M, GPS −20.276547, −43.431717), not affected by Fundão Dam tailings (Figure 1a,b), and the other within the most impacted segment, at the Barra Longa Municipality (GNR-BL, GPS −20.286118, −43.065917) (Figure 1a–c). Fieldwork on both sites of the Gualaxo do Norte River was performed on 14 November 2016, during the wet season. Sediment samples to use as inocula were also collected from the Doce River in the Governador Valadares Municipality (DR-GV, GPS −18.915528, −41.995869) on 28 July 2017, during the dry season (Figure 1a–d). The sampling site not affected by Fundão Dam tailings (GNR-M) is approximately 6.5 km upstream of the point of entry of the tailings in the Gualaxo do Norte River, whereas our sampling site most affected (GNR-BL) is approximately 47 km downstream. The sampling site at the Doce River (DR-GV) is approximately 337 km downstream of the Fundão Dam.

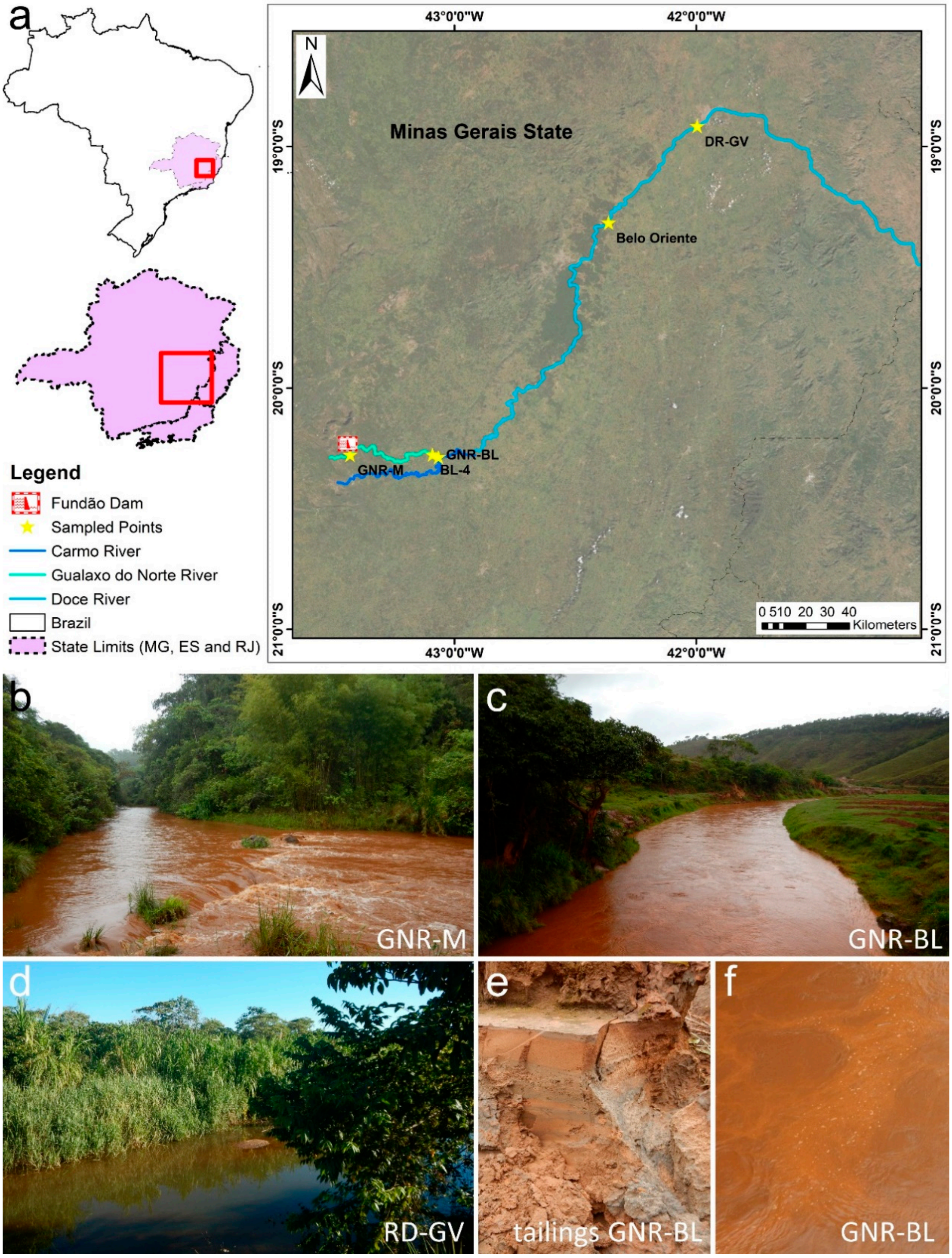

Figure 1. Maps and photographs of the sites from where sediment samples were collected. (**a**) Maps of Brazil and the states of Minas Gerais, Espírito Santo, and Rio de Janeiro and a satellite image illustrating the localization of the Fundão Dam and the sampling points in the Doce River and its tributary the Gualaxo do Norte River. GNR-M, Gualaxo do Norte River in the Mariana Municipality, upstream of the impacted area (**b**). This point reflects the local geology along with iron, manganese, and gold exploitation in its watershed. GNR-BL, Gualaxo do Norte River at the Barra Longa Municipality, within the most impacted area (**c**). DR-GV, Doce River at the Governador Valadares Municipality, less affected by iron mining tailings (**d**). Bottom sediments were also collected at Belo Oriente. Point BL-4 shows a sampling point of Valeriano et al. [53], which is close to GNR-BL. (**e**) Tailings deposited at the banks of the Gualaxo do Norte River after Fundão Dam failure, from where tailing samples were collected. (**f**) Water surface showing the uncommon froth at GNR-BL. Pictures taken in the wet (**b**,**c**,**e**,**f**) and dry (**d**) seasons. Note the distinct appearance of the river water in the impacted (**c**,**f**) and not impacted (**b**) sites of the Gualaxo do Norte River and in the Doce River (impacted) during the dry season (**d**).

Tailings deposited on the Gualaxo do Norte River (GNR-BL) banks during the flood caused by Fundão Dam failure were collected on 1 December 2017, approximately one year after flooding (Figure 1e). River sediments enriched in mine tailings were also collected from the Doce River at Cachoeira Escura (Belo Oriente-MG, GPS −19.31549, −42.36236) in July 2016 (Figure 1a). These materials consist mainly of mine tailings, with some river sediments stirred during flooding that followed the Fundão Dam failure.

For the enrichment cultures, a freshwater (FWA) medium was prepared according to Lovley and Phillips [8]. The medium contained, in grams per liter of distilled water: $NaHCO_3$, 2.5; $CaCl_2$, 0.755; KCl, 0.1; NH_4Cl, 1.5; NaH_2PO_4, 0.74; and $NaCH_3COO$, 6.8. The pH was 8.5. A vitamin solution filtered through a 0.22 µm pore filter was added to the autoclaved medium in a proportion of 1:100 [61]. Synthetic Fe(III) oxide was prepared from the alkalinization of an $FeCl_3$ suspension with NaOH, followed by several cycles of decantation and washing with distilled water, as in McLaughlin et al. [62].

Two distinct strategies were used for the enrichment of Fe(III)-reducing microorganisms. In short-term enrichment cultures, 9 mL glass tubes were filled with 1 mL of inoculum, and 8 mL of the medium containing either synthetic Fe(III) oxide or tailings was collected from the banks of the Gualaxo do Norte River at the Barra Longa Municipality (Figure 1e). The mineral composition of the tailings was assumed to be similar to the BL-4 samples in Valeriano et al. [53], which were obtained from a site close to our sampling site. Fe(III) was 11 g/L in the synthetic Fe(III) oxide medium and 68 g/L in the tailing medium. The enrichment cultures were incubated in the dark at 25 °C for 7, 14, 21, or 28 days. For measurement of Fe(II) concentrations in the liquid phase, 1.35 mL of the liquid phase was retrieved carefully with a micropipette to avoid resuspension of the solid phase and acidified to 1 M HCl within 30 s after opening each tube. Six tubes were used for each time point.

For long-term experiments, FWA medium containing amorphous iron oxide at 5.8 g/L Fe(III) was purged with O_2-free N_2 and dispensed in 50 mL serum bottles, immediately sealed with rubber stoppers and aluminum crimps, and then autoclaved. After cooling, each bottle was inoculated with 4 mL of river sediment. Control samples were autoclaved just after inoculation. All bottles were incubated at 25 °C in the dark.

Fe(II), Fe(III), and total Fe quantification was performed with the ferrozine method, modified from Viollier et al. [63]. Briefly, to 1 mL of the acidified sample, we added 0.2 mL of 0.01 M ferrozine in 0.1 M ammonium acetate, 0.5 mL of 5 M ammonium acetate buffer at pH 9.5, and 0.3 mL of distilled water. For Fe(total) quantification, 0.3 mL of 1.4 M hydroxylamine hydrochloride in 2 M HCl was added after ferrozine solution and allowed to stand for 10 min to fully reduce Fe(III) to Fe(II) before adding ammonium acetate buffer. No water was added for Fe(total) quantification. The absorbance was read at 562 nm in a spectrophotometer. Fe(III) concentrations were calculated as the difference between Fe(total) and Fe(II) concentrations. For quantification of synthetic amorphous Fe(III) oxides and tailing samples used as Fe(III) sources in our enrichment cultures, 0.5 g of dry material was dissolved in 40 mL of 10 M HCl and left for 25 days, diluted, and measured as described above.

Denaturing gradient gel electrophoresis (DGGE) was used to analyze the bacterial communities present in each enrichment. To reach this objective, the total DNA of the microbial community in each enrichment culture was obtained through the DNA extraction method described by Jurelevicius et al. [64]. Briefly, the microbial cells of each sample were lysed using a combination of lysozyme (1 mg/mL) and alkaline lysis buffer from a FastDNA spin kit for soil (QBIOgene, Carlsbad, CA, USA). Then, the DNA was purified according to the methods of Pitcher et al. [65] and subsequently eluted in 50 µL of TE (10 mM Tris-HCl, 0.1 mM EDTA, pH 8.0). The amount of DNA extracted from each sample was determined using a NanoDrop 1000 apparatus (Thermo Scientific, Suwanee, GA, USA). Then, fragments of the 16S rRNA gene from the crude enrichment culture DNA were PCR-amplified using the primers U968F-GC (5 = −G + C clamp-GAACGCGAAGAACCTTAC-3′) and L1401R (5′-CGGTGTGTACAAGACCC-3′) in a 25 µL reaction mixture, as previously described [64].

DGGE of the PCR products was performed using the DCode universal mutation detection system (Bio-Rad DCode, Richmond, VA, USA). Then, 9% (*w/v*) polyacrylamide gels were formulated with a denaturing gradient ranging from 40% to 65%. After electrophoresis, the gels were stained with SYBR Gold nucleic acid gel stain (Molecular Probes, Leiden) for 40 min and then scanned using a Storm PhosphorImager (Amersham Biosciences, Uppsala, Sweden). Analysis of the DGGE profiles was performed using the BioNumerics version 5.10 software package (Applied Maths, St-Martens-Latem, Belgium). The richness (Chao1), diversity (Shannon index), and dominance indices of the bacterial community present in each sample were calculated based on band patterns. The structure of the bacterial community was clustered by nonmetric multidimensional scaling (NMDS) with Bray–Curtis distance using PAST 4.03 software [66]. The significance of the NMDS analysis was compared using the non-parametric multivariate statistical test PERMANOVA [67].

For powder X-ray diffraction (XRD) analysis, samples were washed in acetone to remove organic debris and dried. The material deposited from synthetic Fe(III) oxide was spread on a zero-background cleaved Si wafer support and measured in a D8 Advance Eco instrument (Bruker-AXS, Karlsruhe, Germany) using a Cu Ka source and a position-sensitive LynxEye XE detector with energy discrimination. The samples derived from the long-term crude cultures were ground in a McCrone mill with agate grinding media in water, dried at 60 °C, and backloaded into sample holders for analysis in D4 Endeavor equipment (Bruker-AXS, Karlsruhe, Germany) using a Kβ-filtered Co Ka source and a position-sensitive LynxEye detector. Quantitative phase analysis by the Rietveld method was performed on the latter spectra with Topas v.6 software, also from Bruker-AXS (Karlsruhe, Germany).

For transmission electron microscopy (TEM), samples were put onto Formvar-coated nickel grids, air-dried, and observed under a Jeol JEM 1200 EX transmission electron microscope (Jeol Ltd., Tokyo, Japan). Particle sizes were measured on TEM micrographs using ImageJ software (NIH—National Institutes of Health, Stapleton, NY, USA).

For evaluation of the magnetic properties of the solid phase of long-term cultures, a physical property measurement system (Quantum Design PPMS DynaCool) was used. Zero-field-cooling (ZFC) and field-cooling (FC) magnetization curves were performed with applied magnetic fields of 100 Oe and 1 kOe. In ZFC and FC measurements, data were acquired during warming up from 5 K to 400 K. Magnetic hysteresis loops were performed at temperatures of 10 K, 100 K, 200 K, and 300 K and in magnetic fields ranging from -2 T to 2 T.

Graphs and statistical analyses of Fe(II) quantification, nanoparticle size measurements, and magnetic property evaluation were performed in Microcal Origin 6.0 software (OriginLab, Northampton, MA, USA).

Table 1 summarizes the experiments performed and the analytical tools used.

Table 1. Summary of the experiments. Codes in italic represent samples that changed significantly at the end of the experiment and were further characterized by XRD, transmission electron microscopy, and magnetic property analyses.

Length of the Experiment	Fe(III) Source	Presence of Tailings in the Inoculum	Replicates	Code *	Appearance of the Solids at the End of Incubation		Analytical Methods
					Color	Interaction with Magnets	
Short term (0, 7, 14, 21, and 28 days)	Synthetic	−	6	GNR-M	Rust	Weak	Fe(II) quantification in the liquid phase using the ferrozine assay
		++	6	GNR-BL	Rust	Weak	
		+	6	DR-GV	Rust	Weak	
	Tailings	−	6	GNR-M	Gray	Weak	
		++	6	GNR-BL	Gray	Weak	
		+	6	DR-GV	Gray	Weak	

Table 1. *Cont.*

Length of the Experiment	Fe(III) Source	Presence of Tailings in the Inoculum	Replicates	Code *	Appearance of the Solids at the End of Incubation		Analytical Methods
					Color	Interaction with Magnets	
Long term (170 days)	Synthetic	–	A	sGNR-M-A	Rust	Weak	DGGE
			B	(s)GNR-M-B	Black	Strong	DGGE, XRD, TEM, SQUID
			C	(s)GNR-M-C	Black	Strong	
		++	A	(s)GNR-BL-A	Black	Strong	
			B	sGNR-BL-B	Rust	Weak	DGGE
			C	sGNR-BL-C	Rust	Weak	
	Tailings	–	3	tGNR-M	Gray	Weak	DGGE
		++	3	tGNR-BL	Gray	Weak	

* GNR, Gualaxo do Norte River; M, inoculum collected from a point of the river not affected by Fundão Dam tailings at the Mariana Municipality; BL, inoculum collected from a point of the river heavily affected by Fundão Dam tailings at the Barra Longa Municipality; DR, Doce River; GV, inoculum collected from a point of the Doce River affected by Fundão Dam tailings at the Governador Valadares Municipality; t, tailings; s, synthetic Fe(III) source; A, B, and C represent replicates. The numbers in the Replicates column indicate the number of replicates in experiments where they were not individualized. For each experiment, there was a corresponding dead control with autoclaved inoculum.

3. Results

3.1. Fe(II) Concentrations over Time in the Liquid Phase of Short-Term Cultures

The Fe(II) concentrations in the liquid phase of the short-term enrichment cultures increased in the first three weeks in crude enrichment cultures inoculated with sediment samples containing mining tailings from the Fundão Dam (RD-GV and GNR-BL) in contrast to the control cultures inoculated with autoclaved sediment, where Fe(II) concentrations remained rather stable (Figure 2a,b). Differences between cultures inoculated with living and autoclaved inocula were statistically significant (Student's t-test, $p < 0.01$). Fe(II) concentrations in the liquid phase of enrichment cultures containing either synthetic Fe(III) oxides or tailings as Fe(III) sources were similar in cultures inoculated with sediments from DR-GV ($p > 0.05$; Figure 2a). On the other hand, those inoculated with GNR-BL sediments showed slightly but significantly lower Fe(II) concentrations in cultures using synthetic Fe(III) oxide compared to cultures containing tailings as the Fe(III) source ($p < 0.01$). The increase in soluble Fe(II) concentrations in the crude enrichment cultures indicates the growth of microorganisms able to directly (or indirectly) reduce Fe(III) from both synthetic Fe(III) oxide and Fe(III) oxyhydroxides from tailings.

In cultures using inocula from the Gualaxo do Norte River in the Mariana Municipality (GNR-M) not affected by Fundão Dam tailings, Fe(II) concentrations increased in the first three weeks relative to controls in cultures containing tailings as Fe(III) sources but only in the first week in cultures containing synthetic Fe(III) oxide (Figure 2c). Differences were significant between experimental and control cultures in the first three weeks for cultures using tailings as Fe(III) sources and only in the first and second weeks for cultures containing synthetic, amorphous Fe oxides ($p < 0.01$). Student's t-test showed no significant differences at the $p < 0.01$ level in Fe(II) concentrations of GNR-M cultures using tailings or amorphous Fe(III) oxide as Fe(III) sources, which would be due to the high variability between individual samples, as expressed in the SD bars. Our results indicate Fe(III) reduction to Fe(II) in cultures inoculated with sediments not affected by tailings from the Fundão Dam, although the results were not as robust as in the cultures inoculated with sediments containing tailings. Despite differences in the Fe(II) concentrations in the liquid phase, both the synthetic amorphous Fe(III) oxide and the natural crystalline iron oxides from tailings could be reduced and dissolved by the activities of microorganisms from our three sampling sites.

The pH values remained at approximately 8.5–9.0 in the liquid phase of all tubes during the whole experiment, regardless of the iron source, the inoculum, and the presence of living cells, excluding the possibility of mineral dissolution due to low pH.

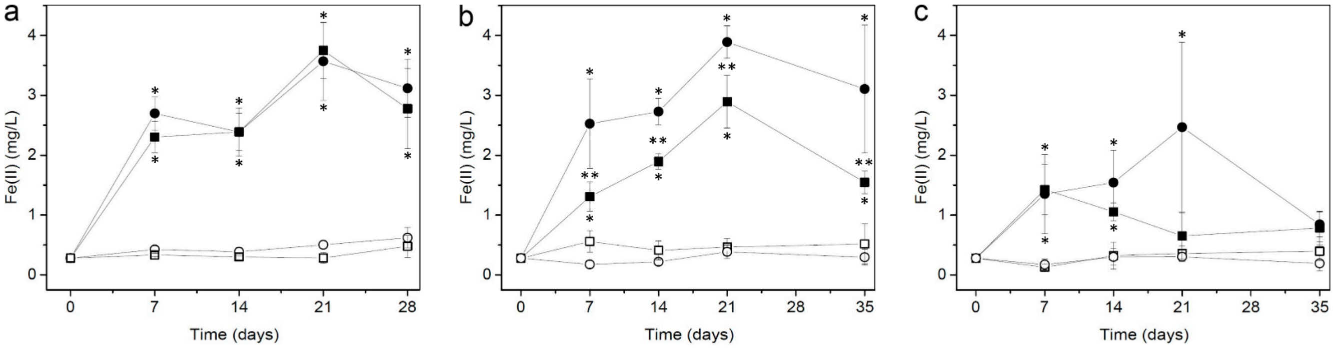

Figure 2. Fe(II) concentrations over time in the liquid phase of enrichment cultures. The iron sources for the cultures were either tailings (circles) or amorphous Fe(III) oxide (squares); closed symbols refer to the experimental, living enrichment cultures, and open symbols refer to control experiments using an autoclaved sediment as the inoculum. Bars show the standard deviation. Asterisks indicate statistical significance between experimental and control cultures (*) or between the two Fe(III) sources (**) (Student's *t*-test, $p < 0.01$). Inocula were obtained from (**a**) the Doce River in the Governador Valadares Municipality (DR-GV), affected by tailings; (**b**) the Gualaxo do Norte River in the Barra Longa Municipality (GNR-BL), highly affected by tailings; and (**c**) the Gualaxo do Norte River in the Mariana Municipality (GNR-M), not affected by tailings from the Fundão Dam.

3.2. Long-Term Cultures and the Presence of Magnetite ($FeO{\cdot}Fe_2O_3$) in the Solid Phase

To clarify whether DIRMs were present in river sediments and the possibility of precipitation of Fe(II) minerals in the enrichment cultures, we prepared 50 mL of long-term crude enrichment cultures and waited for visible changes in the solid phase. The culture media of long-term cultures showed a slight increase in turbidity in the first month (Figure 3a,b). Microbial growth was ascertained by Gram staining of the liquid phase after 20 days, showing mainly Gram-negative rods, most ranging from 3.2 to 4.2 µm in length and 1.0 to 1.3 µm in width. Furthermore, in half of our long-term cultures (three out of six), the solid phase became black and more responsive to applied magnetic fields with time. At 170 days, the black magnetic material seemed to have entirely substituted the synthetic, amorphous Fe oxide used as the Fe(III) source (Figure 3c), and we stopped the experiment to retrieve samples for PCR-DGGE, X-ray diffraction, transmission electron microscopy, and magnetic measurements.

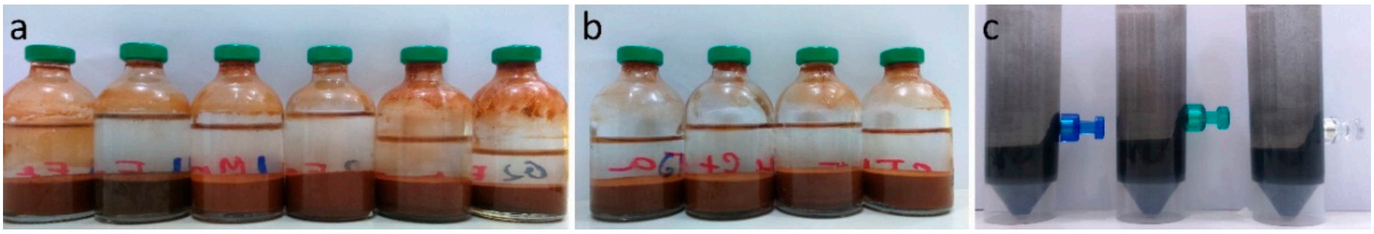

Figure 3. Evolution of the solid phase of long-term enrichment cultures containing synthetic Fe(III) oxyhydroxides as the Fe(III) source. Inocula were obtained from the Gualaxo do Norte River affected (GNR-BL) or not (GNR-M) by tailings from the Fundão Dam. (**a**) Cultures 20 days old. From left to right: GNR-M-A, GNR-M-B, GNR-M-C, GNR-BL-A, GNR-BL-B, and GNR-BL-C. Note the darker color of the second flask (GNR-M-B). (**b**) Control (autoclaved) cultures 20 days old, where the solid phase shows a uniform rust color. (**c**) Solid phase retrieved after 170 days of incubation, showing magnetic minerals attracted to small, strong magnets. The magnetic interaction energy is sufficient to maintain the magnets suspended on the flask walls. From left to right, the samples are GNR-M-B, GNR-M-C, and GNR-BL-A.

Analysis of DGGE patterns obtained from PCR products showed that the microbial populations could be grouped by inoculum origin, as well as by Fe(III) source (Figure 4). The cultures using tailings were grouped closer, indicating an influence of this Fe(III) source on microorganism selection. Interestingly, the cultures that produced the black magnetic material at the end of the experiment could also be grouped together. In these samples, we observed a decrease in both bacterial richness and diversity (Figure 4).

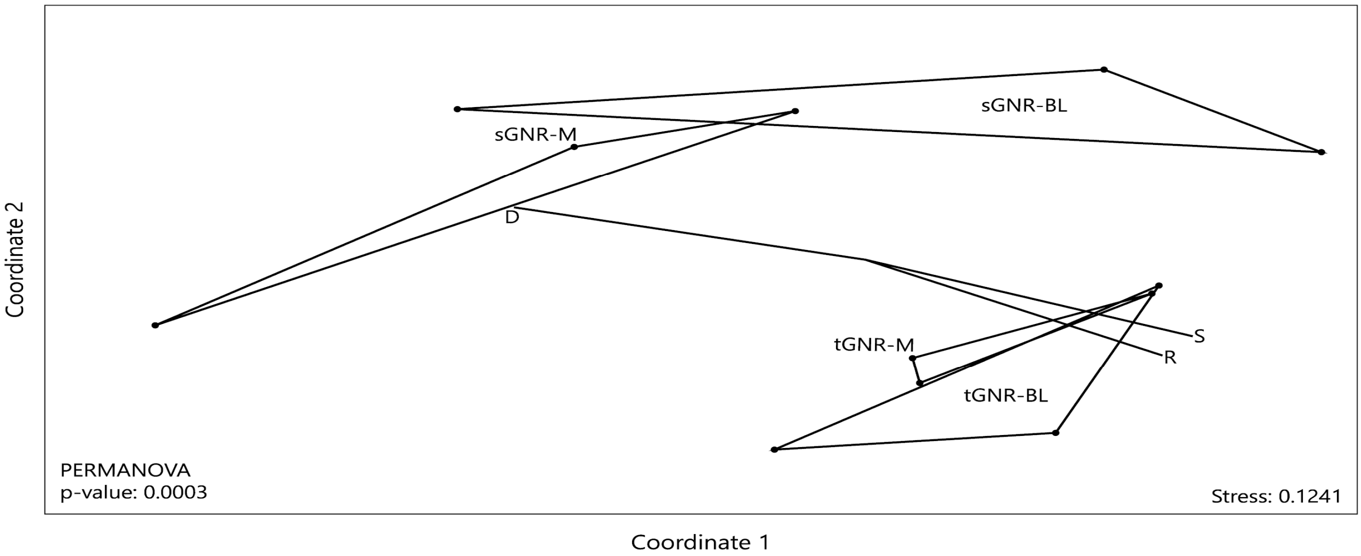

Figure 4. A nonmetric multidimensional scaling (NMDS) ordination diagram based on the denaturing gradient gel electrophoresis (DGGE) fingerprint data obtained from samples of long-term crude cultures. The data were plotted connecting the triplicates of each sample type. The alpha-diversity indices of richness (R), diversity (S), and dominance (D) were used as vectors in this analysis. GNR-M, inocula collected at the Gualaxo do Norte River in the Mariana Municipality, not affected by Fundão Dam tailings; GNR-BL, inocula collected at the Gualaxo do Norte River in the Barra Longa Municipality, affected by Fundão Dam tailings; t, tailings used as the Fe(III) source; s, synthetic, amorphous Fe(III) oxide used as the Fe(III) source.

X-ray diffraction showed that the Fe(III) source consisted of amorphous phases, along with poorly crystalline akaganeite and goethite (Figure 5a). In contrast, the solid, black material that developed in half of the long-term cultures showed increased crystallinity, with magnetite as the main crystalline Fe-bearing component (Figure 5b–d and Table 2). In addition to magnetite, they contained minor amounts of the Fe(III) oxides hematite and goethite, as well as quartz, muscovite, kaolinite, and fluorapatite (Figure 5b–d and Table 2).

Table 2. Rietveld analysis of the solid phase of long-term crude cultures using synthetic Fe(III) oxide as the Fe(III) source, which became black and magnetic after 170 days.

	Wt % Rietveld	
Phase Name	**GNR-M-B ***	**GNR-BL-A ***
Magnetite	52.9	57.1
Goethite	7.1	6.1
Hematite	2.1	2.6
Quartz	16.3	24.8
Muscovite	8.4	7.5
Kaolinite	0.9	1.9
Illite	12.0	0.0

* See Table 1 for details on these samples.

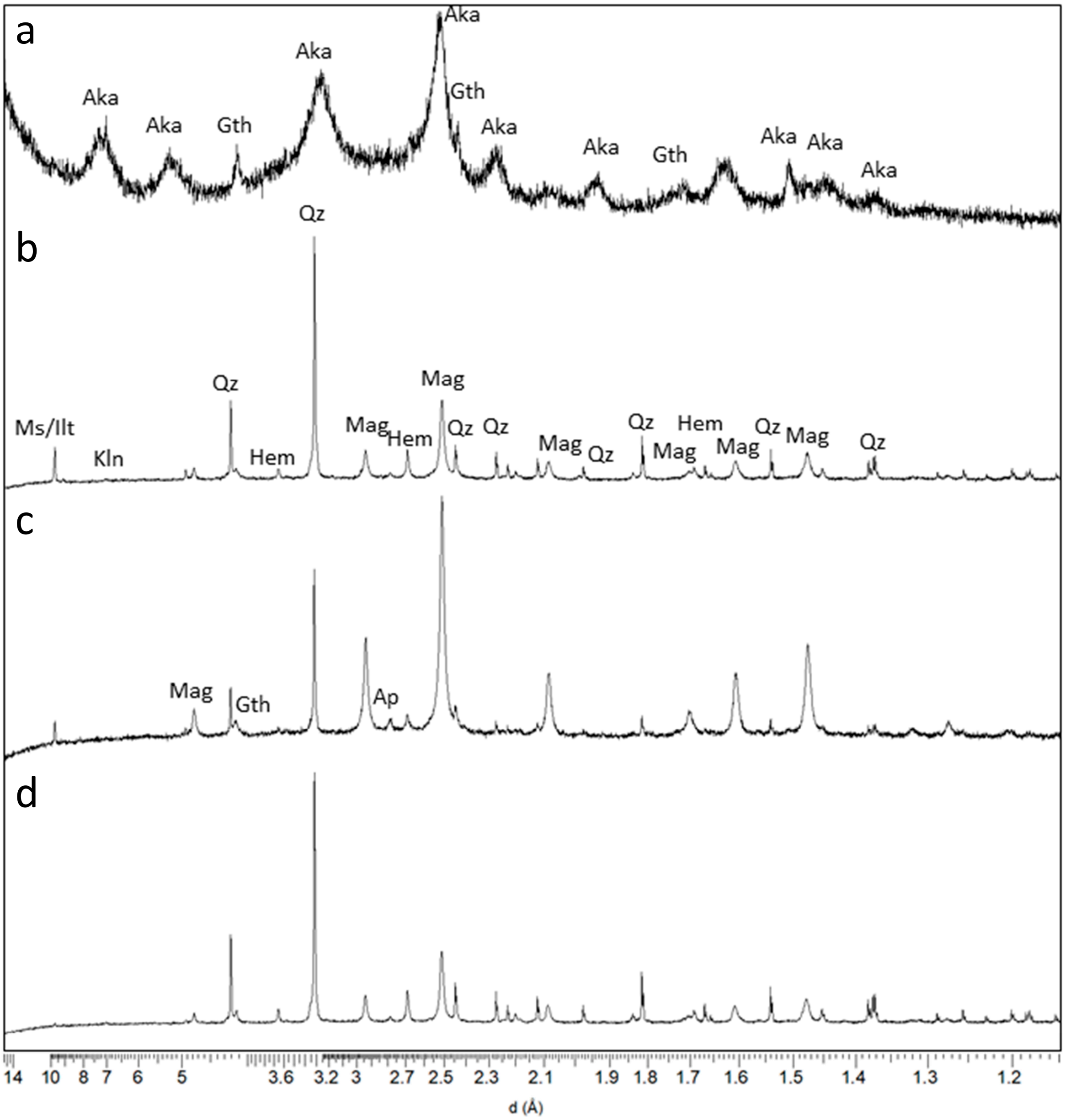

Figure 5. X-ray diffraction of the solid phase of long-term enrichment cultures using the synthetic Fe(III) source. (**a**) Synthetic Fe(III) oxide used as an iron source for enrichment cultures. A pronounced amorphous hump (from ~6 to 2 Å) points to the predominance of amorphous phases, with crystalline akaganeite ($Fe_{3+8}(OOH)_{16}Cl_{1.25} \cdot nH_2O$, Aka) and goethite (FeOOH, Gth) as minor phases. (**b**–**d**) Solid phase of enrichment cultures that turned black and magnetic after 170 days, showing mainly crystalline, mixed-valency iron oxide magnetite ($FeO \cdot Fe_2O_3$) with a diagnostic peak at ~2.53 Å. Other crystalline phases include the common riverine sediment minerals quartz (Qz), muscovite/illite (Ms/Ilt), kaolinite (Kln), fluorapatite (Ap), and the iron oxides hematite (Hem) and goethite (Gth). (**b**) GNR-M-B, (**c**) GNR-M-C, and (**d**) GNR-BL-A. See Table 1 for more details on these samples.

In addition to magnetite, long-term cultures showed minor amounts of the Fe(III) oxides hematite and goethite, as well as quartz, muscovite, kaolinite, and fluorapatite (Figure 5b–d and Table 2), which are common in riverine sediments [68]. Except for fluorapatite, which was present in minor amounts, these minerals were identified in Fundão Dam tailings [51,53,58]. Goethite reflections could also be due to remains of the synthetic Fe(III) oxide used as an Fe(III) source in the enrichment cultures (see Figure 5a) or due to precipitation induced by DIRM activities, as shown before [26,36,40,42,43,45].

Transmission electron microscopy of control (autoclaved) cultures showed tiny, elongated nanoparticles after 170 days (Figure 6a). In contrast, the black solid phase of living cultures contained mainly larger, isotropic particles (Figure 6b–d). Smaller particles were rounded, whereas larger particles showed short prismatic or octahedral morphologies characteristic of magnetite nanocrystals (Figure 6b–d), which was the main mineral identified by X-ray diffraction (Figure 5). Isotropic particles showed a whole size and shape series, from small and rounded to large and euhedral crystals. The width-to-length ratio is rather stable throughout their size range (Figure 7). The presence of twins was relatively common (e.g., Figure 6d, asterisks). For comparison, the morphologies of magnetite produced by pure cultures of DIRMs include euhedral crystals with prismatic, cubic, or rhombic shapes [37], prismatic shapes with frequent twinning [34], or irregular, rounded crystals showing rough surfaces and crystalline defects [69]. Isotropic crystals in our samples were 28–35 nm in average length and 21–24 nm in average width, reaching 177 × 102 nm, with an average width-to-length ratio of 0.74–0.78 (Table 3), which is within the size range previously shown for magnetite produced by DIRM pure cultures, which ranged from 6 to 200 nm in length [24,34,36,37,69].

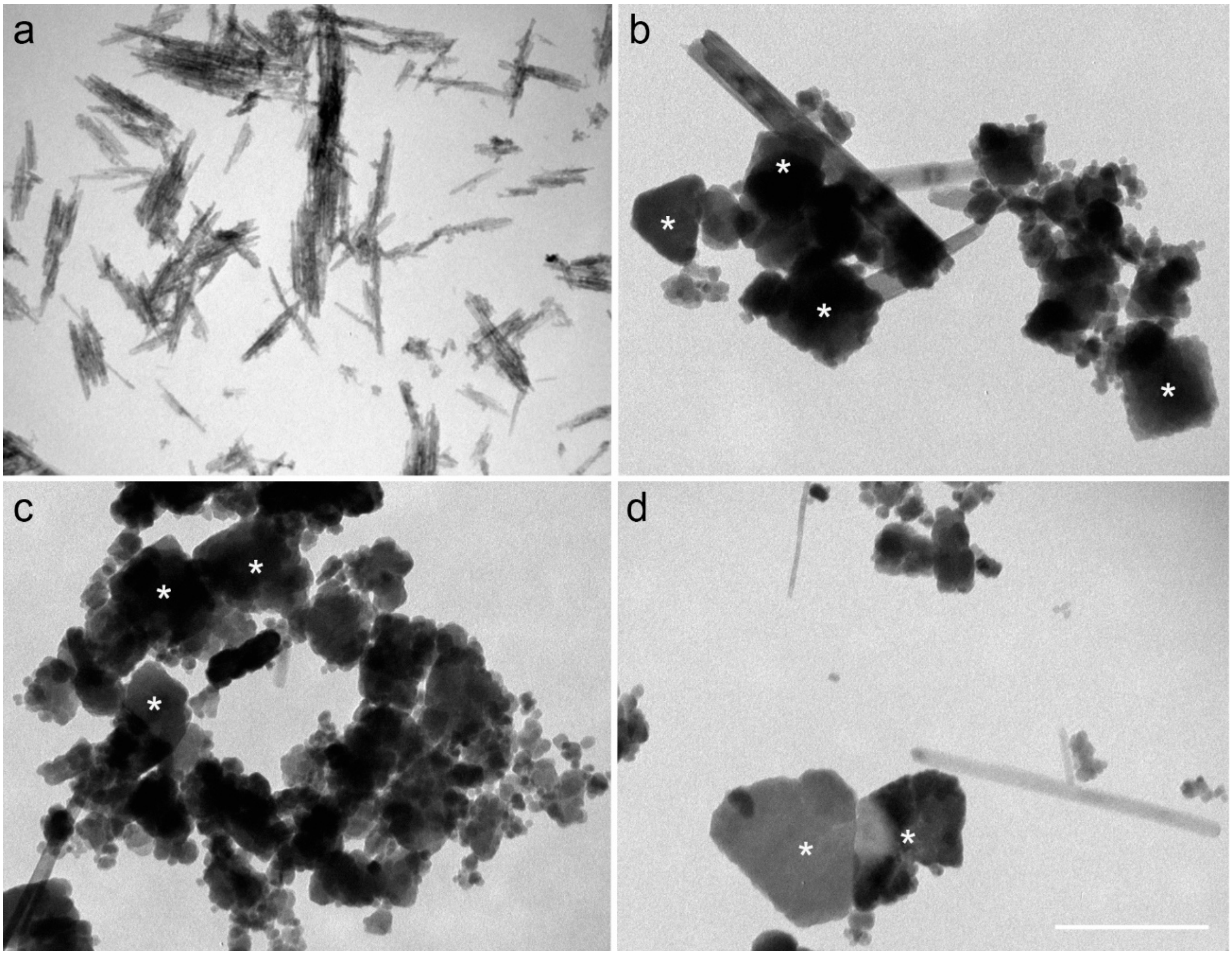

Figure 6. Transmission electron micrographs of the solid phase of enrichment cultures using the synthetic Fe(III) source, showing the evolution of mineral morphologies after 170 days. (**a**) Sample from control (autoclaved) cultures, showing the predominance of elongated nanoparticles. (**b**–**d**) Samples of the black magnetic material that developed in half of the living cultures, showing larger particles, some with octahedral morphologies compatible with magnetite (asterisks). Elongated, lath-shaped crystals were less common than octahedra and other equidimensional particles. (**b**) GNR-M-B, (**c**) GNR-M-C, and (**d**) GNR-BL-A. For more details on samples, see Table 1. Scale bar = 200 nm.

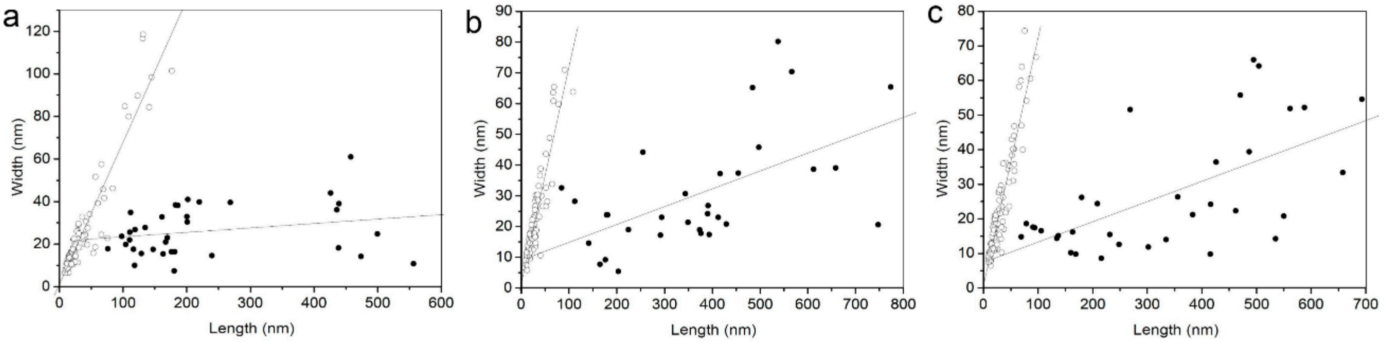

Figure 7. Length/width plots of minerals from the black magnetic solids produced in long-term enrichment cultures retrieved after 170 days. Open circles, isotropic crystals; closed circles, lath-shaped, anisotropic crystals. Note a clear shape distinction between these two minerals, as indicated by the linear fits. (**a**) GNR-M-B, (**b**) GNR-M-C, and (**c**) GNR-BL-A. See Table 1 for more information on the samples.

Table 3. Size and shape factor of crystalline particles observed by transmission electron microscopy.

Crystal Shape	Sample	Length (nm) (Average ± SD)	Length Range (nm)	Width (nm) (Average ± SD)	Width Range (nm)	Width/Length	N
Isotropic (octahedral, prismatic, or rounded)	GNR-M-B *	35 ± 34	9–177	24 ± 24	7–119	0.74 ± 0.17	100
	GNR-M-C *	28 ± 18	7–108	21 ± 14	7–71	0.78 ± 0.15	100
	GNR-BL-A *	29 ± 19	9–96	22 ± 14	8–74	0.76 ± 0.16	112
Elongated (lath shaped)	GNR-M-B *	229 ± 139	76–556	26 ± 12	18–61	0.14 ± 0.07	35
	GNR-M-C *	371 ± 181	84–774	31 ± 19	33–80	0.10 ± 0.07	31
	GNR-BL-A *	329 ± 184	69–693	26 ± 17	15–64	0.10 ± 0.06	34

* Samples of black and magnetic solids produced in crude cultures. See Table 1 for more details.

In addition to the isotropic crystals, smaller numbers of long, lath-shaped crystals occurred in all three black magnetic samples (Figure 6b–d). These were apparently monocrystalline, as inferred by the diffraction contrast and/or Moiré patterns observed in the microscope, reaching 774 nm in length (average 229–371 nm) and up to 80 nm in width (average 26–31 nm) (Table 3). Width-to-length ratios averaged 0.01 to 0.14. Figure 7 confirms the presence of two types of particles, distinct in size and shape, in each of the three samples. The morphology of isotropic crystals is rather stable throughout their size range, whereas lath-shaped crystals are more variable in shape. Because these shapes were absent from both the Fe(III) source sample (not shown) and autoclaved cultures (dead controls; see Figure 6a), we think that such crystals resulted from microbial activities. Similar lath-shaped crystals from DIRM pure cultures have been identified as goethite [19,20,45]. This shape similarity, as well as the presence of goethite reflections in XRD of the three samples (Figure 5 and Table 2), indicates that these lath-shaped crystals consist of goethite. Although goethite is a main mineral in tailings and now also in riverine sediments [53], these morphologies were not observed in river sediments (not shown).

The zero-field-cooling (ZFC) and field-cooling (FC) magnetization curves provide information about the blocking temperature, the distribution of blocking temperatures, the size of magnetic domains, magnetic ordering transitions (e.g., Verwey, Morin, spin glass), magnetic interaction, and the chemical composition of magnetic minerals [70]. Figure 8a–c shows the ZFC and FC magnetization curves at an applied magnetic field of 100 Oe. The results suggest that the blocking temperature occurs above 400 K in all samples, given that no maximum was observed in the ZFC curves. The FC curves at low temperatures are almost constant, which would be expected for a system with strong dipolar interactions between the nanoparticles [71,72]. This result is consistent with the TEM observations (Figure 6b–d), which show mainly nanoparticle aggregates. Strong dipolar interactions can modify the energy barrier in superparamagnetic nanoparticles, resulting in an increase in the blocking temperature and a narrowing of the blocking temperature distribution [71]. The divergence of the ZFC and FC curves is characteristic of the existence of a magnetic anisotropy barrier [73].

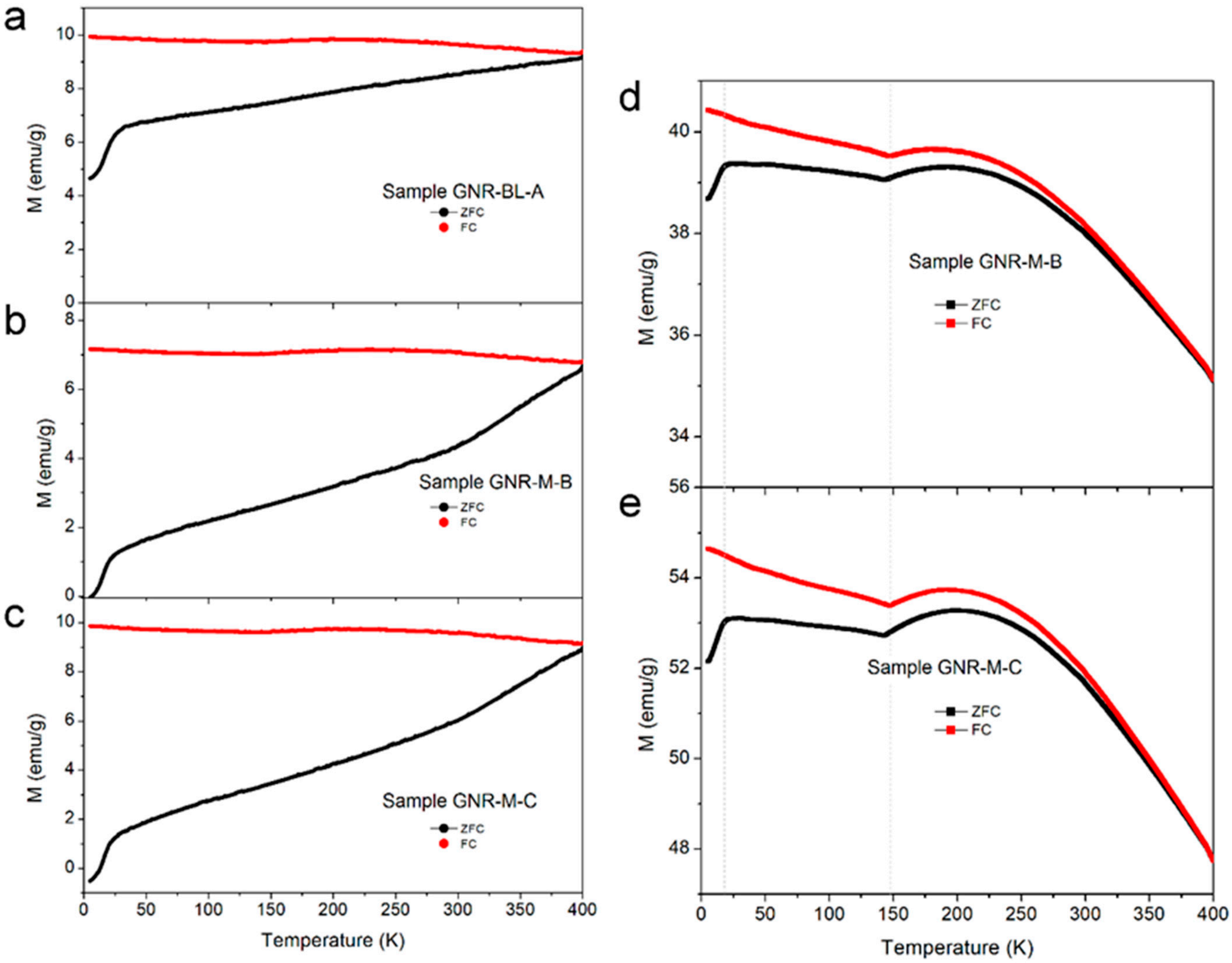

Figure 8. Zero-field-cooling (ZFC) and field-cooling (FC) magnetization curves as a function of temperature obtained from the black and magnetic solid phases of long-term enrichment cultures. Black line, ZFC; red line, FC. (**a**–**c**) Left panel showing ZFC and FC curves obtained at 100 Oe. (**d**,**e**) Right panel showing ZFC and FC curves at 1 kOe. Note transitions at ~30 K (**a**-**e**) and ~150 K (**d**,**e**) and the distinct regimens below and above 150 K at 1 kOe (**d**,**e**). (**a**) GNR-BL-A, (**b**,**d**) GNR-M-B, and (**c**,**e**) GNR-M-C. See Table 1 for more details on these samples.

At low temperatures, a sudden slope in the ZFC curves appears in the three samples, suggesting a possible transition at approximately 30 K (Figure 8). For very small magnetite nanoparticles (~8 nm), a Verwey transition at approximately 30–50 K has been identified [74]. In addition, the magnetic regime at approximately 30 K has been associated with surface spin disorder due to the symmetry breaking of small magnetic nanoparticles of goethite [75,76]. Indeed, both magnetite and goethite were identified in our samples by XRD (Figure 5 and Table 2), and numerous isotropic nanoparticles approximately 8 nm in diameter were observed by transmission electron microscopy (Figure 6b–d and Table 3).

Figure 8d,e shows the ZFC and FC magnetization curves as a function of temperature at a 1 kOe applied magnetic field for samples GNR-M-B and GNR-M-C. This field is strong enough to reveal the blocking temperature, because the magnetic energy decreases the energy barrier between the magnetic states in the magnetic nanoparticle. The ZFC curves show two magnetic regimes, the first one at approximately 30 K, observed in the ZFC curves at both 100 Oe and 1 kOe (Figure 8a–e). The second regime is a broad maximum magnetization observed at approximately 200 K under 1 kOe and can be associated with the blocking temperature of a size distribution of nanoparticles because the blocking temperature shifts for low temperatures with an increase in the applied magnetic field. The ZFC and FC curves suggest that nanoparticles with narrow size distributions overlap above the blocking temperature.

Figure 9 shows the magnetization curves as a function of the magnetic field $M(H)$ at different temperatures (10, 100, 200, and 300 K) in all samples. At room temperature (300 K), no sample showed superparamagnetic behavior. The $M(H)$ curve does not saturate under a magnetic field of 20 kOe. This would be consistent with the presence of goethite and hematite particles [77]. The values of the saturation magnetization were estimated at the 20 kOe magnetic field. The magnetic parameters obtained from $M(H)$ are summarized in Table 4. At lower temperatures, the values of the coercive field were lower than the value reported for magnetite nanoparticles of 17 nm (370 Oe) [72], due to the presence of other magnetic phases in the three samples.

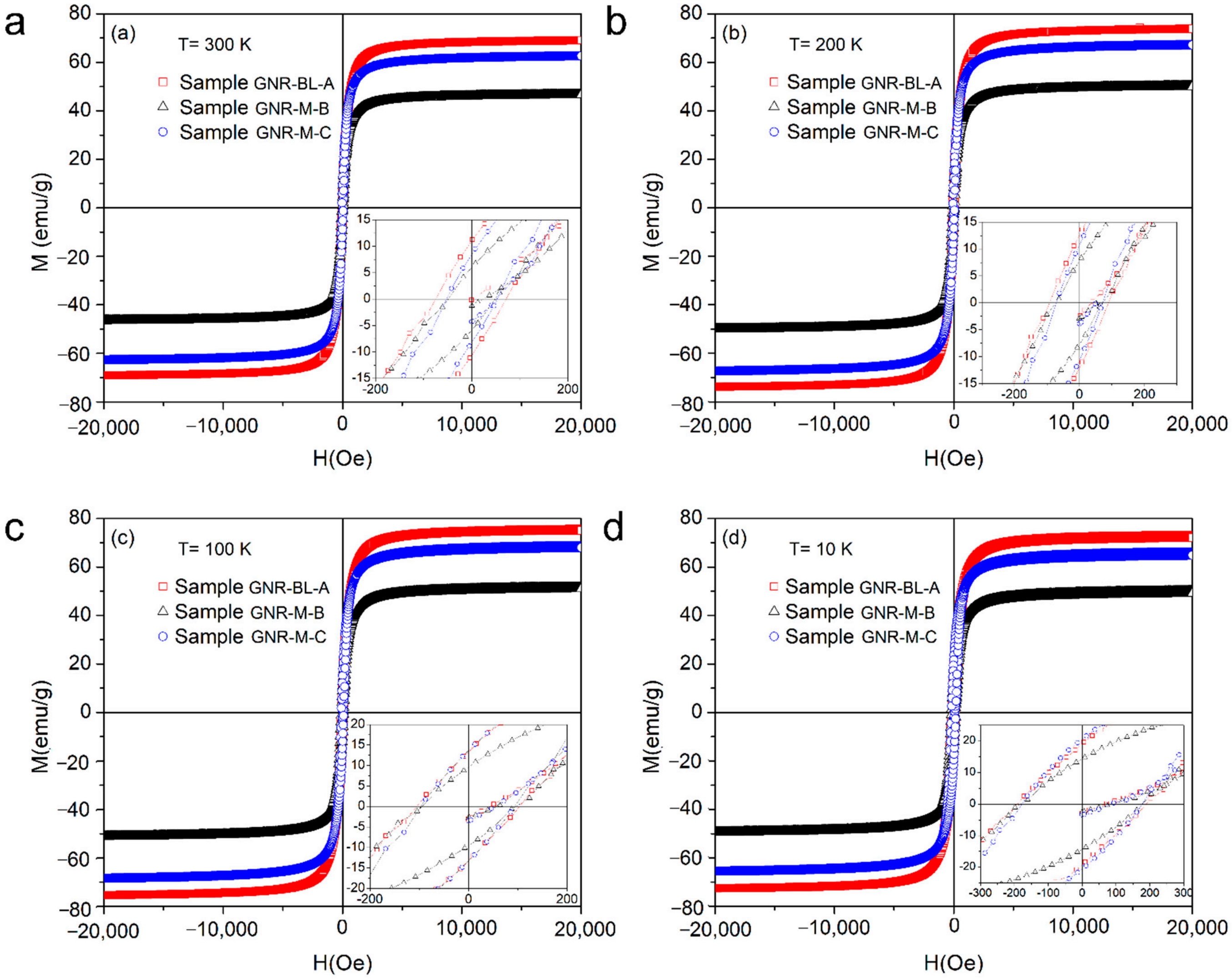

Figure 9. Magnetization as a function of the applied magnetic field at (**a**) 300 K, (**b**) 200 K, (**c**) 100 K, and (**d**) 10 K for samples of black and magnetic solids obtained in the long-term enrichment cultures of GNR-BL-A (red squares), GNR-M-B (black triangles), and GNR-M-C (blue circles). Inserts show the hysteresis curve for low magnetic field values, where it is possible to observe the coercive field and the remanent magnetization. See Table 1 for detailed information on the samples.

Table 4. Magnetic parameters obtained from *M*(*H*) at different temperatures.

Sample	T (K)	H_c (Oe)	M_r (emu/g)	M_s (emu/g)	H_{cr} (Oe)
GNR-BL-A *	300	75 (10)	11.2	69	160 (10)
	200	91 (10)	12.6	74	200 (10)
	100	105 (10	13.3	75	204 (10)
	10	190 (10)	19.7	73	420 (10)
GNR-M-B *	300	50 (10)	5.9	46	115 (10)
	200	73 (10)	7.7	50	140 (10)
	100	96 (10)	9.5	51	180 (10)
	10	180 (10	14.3	50	320 (10)
GNR-M-C *	300	33 (10)	8.3	62	100 (10)
	200	53 (10	10.7	67	140 (10)
	100	71 (10)	13.6	69	183 (10)
	10	177 (10)	20.5	66	370 (10)

* Samples of black and magnetic solids retrieved from crude enrichment cultures after 170 days. See Table 1 for more details. H_c, coercive field; M_r, remanent magnetization; M_s, saturation magnetization; and H_{cr}, coercive remanent field.

A rough estimate of the anisotropy constant was performed using the value of the maximum temperature of the ZFC curve, which is proportional to the blocking temperature ($T_{\max} \approx 2T_B$) [78] observed in the ZFC curve at 1 kOe, by using the following relation [79]:

$$T_B = \frac{K_{eff}V}{25k_B}\left(1 - \frac{H}{H_K}\right)^{3/2} \tag{1}$$

where H_K is the anisotropy field ($H_K = 2K_{eff}/M_s$) and M_S is the saturation magnetization.

Using the volume for the nanoparticles observed by TEM (approximately 12,348 nm^3 and 20,160 nm^3 considering the nanoparticles as parallelepipeds; see data in Tables 3 and 4) and M_s from *M(H)* at 10 K (approximately 50 emu/g and 66 emu/g for GNR-M-B and GNR-M-C samples, respectively), magnetic anisotropies of 1.6×10^5 erg/cm^3 and 2.3×10^5 erg/cm^3 are obtained for GNR-M-B and GNR-M-C samples, respectively. This result is consistent with the magnetic anisotropy values of bulk magnetite (1.35–1.87 $\times 10^5$ erg/cm^3) [80] and nanoparticles [81,82].

The values for the remanence to saturation magnetization rate M_r/M_s calculated from *M*(*H*) at 10 K were 0.27, 0.29, and 0.31 for GNR-BL-A, GNR-M-B, and GNR-M-C, respectively. These values are smaller than 0.5 for noninteracting nanoparticles with random and uniaxial anisotropy [83]. This indicates the presence of interparticle interactions of antiferromagnetic nature [84]. It was noted in all samples at room temperature that the saturation magnetization is lower than the value for bulk magnetite (92 emu/g) [80] due to the presence of an antiferromagnetic phase that could correspond to goethite or hematite (1–2.5 emu/g) or due to disorder on the surface of very small iron oxide nanoparticles [85].

4. Discussion

4.1. Soluble Fe(II) and Magnetite as Proxies for DIRM Enrichment

Both the synthetic amorphous Fe(III) oxide and the natural crystalline iron oxides from tailings could be reduced by microorganisms from our three sampling sites, producing soluble Fe(II) and/or magnetite, as shown before for DIRM pure cultures [8,10,12,18,19,23,24,26,28,30,32–38,40,42]. In fact, the product of dissimilatory iron reduction is Fe(II), which can assume both soluble and solid forms, depending on local conditions [19,31,33,86]. The pH of our cultures remained at approximately 8.5–9.0, which would favor magnetite precipitation [86–88]. Indeed, Fe(II) concentrations reached in the liquid phase of our cultures were low compared to pure DIRM cultures [19] and probably represent a fraction of total Fe(II) produced. Zachara et al. [43] showed that most iron reduced by *Shewanella putrefaciens* cultures precipitated as magnetite, siderite, vivianite, and/or green rust, depending on both medium and headspace composition.

In particular, the production of magnetite from amorphous Fe oxides is a main characteristic of DIRMs [6–8,10,12,13,15]. Magnetotactic bacteria are also known to produce magnetite, but magnetite occurs intracellularly, and the yield is much lower [89] (compare Lovley et al. [32] with Berny et al. [90]). Thus, our results show that DIRMs are present in the sediments of the Gualaxo do Norte River affected and not affected by mining tailings from the Fundão Dam and that they could be cultured using enrichment techniques.

4.2. Significance of Soluble Fe(II) and the Crystalline Phases Magnetite, Goethite, and Hematite in Crude Enrichment Cultures

Several wet-chemistry pathways for magnetite precipitation at room temperature involve the reaction of soluble Fe^{2+} ions with solid Fe(III) phases, such as akaganeite, goethite, lepidocrocite, hematite, and/or maghemite, with the reduction of Fe(III) minerals by soluble Fe^{2+} and topotactic reactions playing key roles in transforming Fe(III) phases into magnetite [88,91,92]. Our synthetic Fe(III) source consisted of goethite, akaganeite, and amorphous phase(s), whereas magnetite, goethite, and hematite were the Fe oxyhydroxides found after 170 days in half of our long-term cultures. Our TEM images showed that the tiny anisotropic particles observed in control cultures were substituted for larger crystalline particles showing two distinct shapes: isotropic crystals, which probably correspond to magnetite (and perhaps also some hematite), and anisotropic, long, and thin crystals, probably corresponding to goethite. Despite the fact that goethite was detected in the XRD of the synthetic Fe(III) source (see Figure 5a) and in tailings from the Fundão Dam [53], its shape and size indicate growth within the magnetite-producing cultures. The distinctions in crystallinity, shape, size, and polymorph indicate that dissolution-reprecipitation and/or epitaxial growth had a role in the path from the synthetic Fe(III) source to magnetite. A particularly interesting pathway for wet synthesis of magnetite was proposed by Ahn et al. [91], where (i) poorly crystalline akaganeite was converted to goethite through dissolution and reprecipitation, (ii) goethite turned to hematite by topotactic transformation at the tip of the goethite crystals, and (iii) hematite was partially reduced by soluble Fe^{2+} and turned into magnetite. Accordingly, Vali et al. [34] and Han et al. [26] interpreted goethite and hematite in DIRM cultures as intermediate stages in magnetite synthesis.

4.3. Significance of DIRMs in the Context of Riverine Sediments Enriched in Tailings

Here, we showed that DIRMs are present and active in both Gualaxo do Norte and Doce Rivers in areas impacted and not impacted by mining tailings from the Fundão Dam and that they are able to reduce Fe(III) of crystalline minerals from tailings to Fe(II) using acetate as an electron donor. DNA from known DIRM genera, such as *Geobacter* and *Geothrix*, was found in sediments of the Doce River and its tributary the Carmo River after the Fundão Dam burst [93,94], but it was not shown if they were actively reducing Fe(III) minerals in the river sediments. Although the bottom sediments of the Gualaxo do Norte River stretch impacted by tailings showed very small TOC values [54], the downstream Doce River is impacted by the discharge of untreated sewage [59,60]. Jardim et al. [59] estimated that untreated sewage of approximately 870,000 people was discharged into the Doce River mainstream and tributaries, contributing an estimated 8 tons of organic N and 2.2 tons of organic P per day to the watershed, which led to eutrophication and recurrent cyanobacterial blooms before dam burst [59]. Richard et al. [60] reported excess thermotolerant coliforms in several stretches of the Doce River and tributaries after dam burst, which indicated continuous release of untreated sewage directly into the rivers. In addition, several stretches of the Doce River mainstream showed high BOD (biochemical oxygen demand) and/or low DO, indicating high loads of organics [60]. It is possible that untreated sewage can be a source of organics for DIRM activities.

The Fe(II) produced from the partial reduction of an Fe(III) amorphous phase could either become soluble or precipitate as magnetite. In the environment, the fate of soluble Fe(II) could be to precipitate as authigenic Fe(II) minerals such as magnetite, green rust, siderite, and vivianite, as observed before [29,39,86,95–100]; to react with minerals in soils and sediments [96,101,102]; or, once it diffuses into oxygenated environments, to oxidize and precipitate as secondary Fe(III) oxyhydroxides [96,97,101,103–109], which are frequently associated with indigenous microorganisms [29,103–108].

Fe(III) reduction to Fe(II) by DIRMs frequently leads to mineral dissolution, releasing other elements in addition to iron into the water [30,31,99,102], which could lead to increased concentrations of these elements [102,107]. Furthermore, some DIRMs are able to reduce other elements, changing their solubility [3]. Released trace metals and phosphates can remain in solution [30,95,102]; adsorb to available mineral surfaces [99,102,103,108,110]; and/or coprecipitate with iron in secondary, authigenic Fe(II) and/or Fe(III) minerals [29,95,99,100,102,103,106–109,111]. The problem is that authigenic iron minerals are frequently nanometric, less crystalline, and more reactive than primary minerals, and thus toxic elements bound to such minerals may be easily remobilized [102].

In the fine tailing particles that reached the Doce River estuary, iron oxide fractions contained Co, Cr, Cu, Ni, Pb, and Zn at mg/kg levels, which could be mobilized if the Fe(III) oxides were reduced and dissolved by DIRMs [58]. The same fractionation showed Mn in the g/kg range in the exchangeable and soluble fractions, which are easily mobilized [58]. Several DIRMs are known to reduce Mn(IV) in manganese oxides to soluble Mn(II), which can remain in solution [2,9,110,112]. In addition, Fe^{2+} ions produced by DIRMs can chemically reduce Mn(IV) to Mn(II) [104]. After failure of the Fundão Dam, the concentrations of Fe, Mn, Al, and/or Cd in waters along impacted stretches of the Doce River watershed have increased [56,60,113]. The release of these metals from tailings and other minerals from bottom sediments due to the activities of DIRMs is a probable cause.

The activities of Fe(III)-reducing microorganisms in the Doce River and tributaries raise the possibility of slow dissolution of the huge amounts of primary, highly crystalline iron oxides that remain in the sediments, releasing trace elements adsorbed to mineral surfaces or incorporated into the crystalline lattice, which could impair water quality. The precipitation of secondary, authigenic Fe(II) and/or Fe(III) minerals such as magnetite could incorporate some of them, but this is a very complex issue that depends on several physical, chemical, and biological factors [102,106,107,110]. Moreover, such phases are usually poorly crystalline, highly reactive, and easily redissolved [29,98,101,102,105,106,110,111].

5. Conclusions

DIRMs are present and active in both Gualaxo do Norte and Doce Rivers, in stretches affected or not affected by tailings from the Fundão Dam. They are able to reduce Fe(III) from both synthetic Fe(III) oxide and tailings, producing Fe(II), which can either remain in solution or precipitate as nanocrystalline magnetite ($FeO{\cdot}Fe_2O_3$). Our sampling points were distinct and far away from each other, enabling extension of the conclusions of this work to the whole length of the Doce River and tributaries affected by Fundão Dam tailings.

The implications for the iron-enriched environments of the Doce River and tributaries are related to the fate of tailings over time, as well as to the water quality for human and animal consumption, agriculture, and wildlife preservation. In addition to iron mine tailings, the Doce River watershed is threatened by artisanal gold mining, improper agricultural practices, and discharge of untreated sewage. DIRM activities fueled by organics from sewage and other sources could mobilize iron from Fe oxyhydroxides in the sediments, releasing trace elements in the process. Even though most of the reduced Fe and trace elements could reprecipitate in secondary minerals, such as magnetite ($FeO{\cdot}Fe_2O_3$), the process has the potential to exchange larger, more stable, and crystalline minerals for less crystalline, smaller, and thus more unstable particles.

From the point of view of water quality, probably the best scenario would be a low ratio of Fe(III) reduction in the tailing-enriched sediments, slowing trace metal release into the water column. Because DIRMs are heterotrophic and depend on organic matter, the control of both organic matter input and eutrophication could restrain DIRM activities in the sediments; reduce the concentrations of Al, Cd, Mn, and other trace elements in the water; and improve water quality.

Author Contributions: Conceptualization, C.N.K., D.A.-A., R.N. and D.A.J.; methodology, C.N.K.; validation, C.N.K. and M.F.; formal analysis, C.N.K., J.D.P.S., D.A.-A., R.N. and D.A.J.; investigation, C.N.K., J.D.P.S., D.A.-A., R.N., A.S.S., D.A.J., R.S.P. and P.M.d.S.; resources, C.N.K., D.A.-A., R.N., D.A.J., L.S. and M.F.; data curation, C.N.K., D.A.-A., R.N. and D.A.J.; writing—original draft preparation, C.N.K. and D.A.-A.; writing—review and editing, J.D.P.S., R.N., D.A.J., L.S. and M.F.; visualization, C.N.K., J.D.P.S., D.A.-A., A.S.S., R.N., D.A.J. and R.S.P.; supervision, C.N.K.; project administration, C.N.K. All authors have read and agreed to the published version of the manuscript.

Funding: This research received no external funding.

Data Availability Statement: The data presented in this study are available in the article.

Acknowledgments: We thank Douglas A. Pabst, Daniel Mendes da Silva, and Roberto Keim for help in collecting samples, and to VHR Menezes da Silva for the maps. J.D.P. Serna acknowledges financial support from the "Programa de Capacitação Institucional"—PCI program of the Brazilian agency Conselho Nacional de Desenvolvimento Científico e Tecnológico—CNPq. We also acknowledge CENABIO for electron microscopy facilities.

Conflicts of Interest: The authors declare no conflict of interest.

References

1. Lovley, D.R. Organic matter mineralization with the reduction of ferric iron: A review. *Geomicrobiol. J.* **1987**, *5*, 375–399. [CrossRef]
2. Lovley, D.R. Dissimilatory Fe(III) and Mn(IV) reduction. *Microbiol. Rev.* **1991**, *55*, 259–287. [CrossRef] [PubMed]
3. Lovley, D.R. Dissimilatory metal reduction. *Annu. Rev. Microbiol.* **1993**, *47*, 263–290. [CrossRef]
4. Myers, C.R.; Nealson, K.H. Respiration-linked proton translocation coupled to anaerobic reduction of manganese(IV) and iron(III) in *Shewanella putrefaciens* MR-1. *J. Bacteriol.* **1990**, *172*, 6232–6238. [CrossRef]
5. Weber, K.A.; Achenbach, L.A.; Coates, J.D. Microorganisms pumping iron: Anaerobic microbial iron oxidation and reduction. *Nat. Rev. Microbiol.* **2006**, *4*, 752–764. [CrossRef]
6. Lovley, D.R.; Phillips, E.J.P. Availability of ferric iron for microbial reduction in bottom sediments of the freshwater tidal Potomac River. *Appl. Environ. Microbiol.* **1986**, *52*, 751–757. [CrossRef]
7. Lovley, D.R.; Phillips, E.J.P. Organic matter mineralization with reduction of ferric iron in anaerobic sediments. *Appl. Environ. Microbiol.* **1986**, *51*, 683–689. [CrossRef]
8. Lovley, D.R.; Phillips, E.J.P. Novel mode of microbial energy metabolism: Organic carbon oxidation coupled to dissimilatory reduction of iron or manganese. *Appl. Environ. Microbiol.* **1988**, *54*, 1472–1480. [CrossRef] [PubMed]
9. Venkateswaran, K.; Dollhopf, M.E.; Aller, R.; Stackebrandt, E.; Nealson, K.H. *Shewanella amazonensis* sp. nov., a novel metal-reducing facultative anaerobe from Amazonian shelf muds. *Int. J. Syst. Bacteriol.* **1998**, *48*, 965–972. [CrossRef] [PubMed]
10. Cummings, D.E.; Caccavo Jr, F.; Spring, S.; Rosenzweig, R.F. *Ferribacterium limneticum*, gen. nov., sp. nov., an Fe(III)-reducing microorganism isolated from mining-impacted freshwater lake sediments. *Arch. Microbiol.* **1999**, *171*, 183–188. [CrossRef]
11. Francis, C.A.; Obraztsova, A.Y.; Tebo, B.M. Dissimilatory metal reduction by the facultative anaerobe *Pantoea agglomerans* SP1. *Appl. Environ. Microbiol.* **2000**, *66*, 543–548. [CrossRef] [PubMed]
12. Kostka, J.E.; Dalton, D.D.; Skelton, H.; Dollhopf, S.; Stucki, J.W. Growth of iron(III)-reducing bacteria on clay minerals as the sole electron acceptor and comparison of growth yields on a variety of oxidized iron forms. *Appl. Environ. Microbiol.* **2002**, *68*, 6256–6262. [CrossRef] [PubMed]
13. Iwahori, K.; Watanabe, J.-I.; Tani, Y.; Seyama, H.; Miyata, N. Removal of heavy metal cations by biogenic magnetite nanoparticles produced in Fe(III)-reducing microbial enrichment cultures. *J. Biosci. Bioeng.* **2014**, *117*, 333–335. [CrossRef] [PubMed]
14. Yang, Z.; Shi, X.; Wang, C.; Wang, L.; Guo, R. Magnetite nanoparticles facilitate methane production from ethanol via acting as electron acceptors. *Sci. Rep.* **2015**, *5*, 16118. [CrossRef]
15. Nixon, S.L.; Telling, J.P.; Wadham, J.L.; Cockell, C.S. Viable cold-tolerant iron-reducing microorganisms in geographically diverse subglacial environments. *Biogeosciences* **2017**, *14*, 1445–1455. [CrossRef]
16. Fortney, N.W.; He, S.; Converse, B.J.; Beard, B.L.; Johnson, C.M.; Boyd, E.S.; Roden, E.E. Microbial Fe(III) oxide reduction potential in Chocolate Pots hot spring, Yellowstone National Park. *Geobiology* **2016**, *14*, 255–275. [CrossRef]
17. Kostka, J.E.; Nealson, K.H. Dissolution and reduction of magnetite by bacteria. *Environ. Sci. Technol.* **1995**, *29*, 2535–2540. [CrossRef] [PubMed]
18. Roden, E.E.; Zachara, J.M. Microbial reduction of crystalline iron(III) oxides: Influence of oxides surface area and potential for cell growth. *Environ. Sci. Technol.* **1996**, *30*, 1618–1628. [CrossRef]
19. Zachara, J.M.; Fredrickson, J.K.; Li, S.-M.; Kennedy, D.W.; Smith, S.C.; Gassman, P.L. Bacterial reduction of crystalline Fe^{3+} oxides in single phase suspensions and subsurface materials. *Am. Mineral.* **1998**, *83*, 1426–1443. [CrossRef]
20. Cummings, D.E.; Caccavo, F., Jr.; Fendorf, S.; Rosenzweig, R.F. Arsenic mobilization by the dissimilatory Fe(III)-reducing bacterium *Shewanella alga* BrY. *Environ. Sci. Technol.* **1999**, *33*, 723–729. [CrossRef]
21. Bonneville, S.; Van Cappellen, P.; Behrends, T. Microbial reduction of iron(III) oxyhydroxides: Effects of mineral solubility and availability. *Chem. Geol.* **2004**, *212*, 255–268. [CrossRef]

22. Cutting, R.S.; Coker, V.S.; Telling, N.D.; Kimber, R.L.; van der Laan, G.; Pattrick, R.A.D.; Vaughan, D.J.; Arenholz, E.; Lloyd, J.R. Microbial reduction of arsenic-doped schwertmannite by *Geobacter sulfurreducens*. *Environ. Sci. Technol.* **2012**, *46*, 12591–12599. [CrossRef] [PubMed]
23. Ouyang, B.; Lu, X.; Liu, H.; Li, J.; Zhu, T.; Zhu, X.; Lu, J.; Wang, R. Reduction of jarosite by *Shewanella oneidensis* MR-1 and secondary mineralization. *Geochim. Cosmochim. Acta* **2014**, *124*, 54–71.
24. Till, J.L.; Guyodo, Y.; Lagroix, F.; Ona-Nguema, G.; Brest, J. Magnetic comparison of abiogenic and biogenic alteration products of lepidocrocite. *Earth Planet. Sci. Let.* **2014**, *395*, 149–158. [CrossRef]
25. Castro, L.; Blásquez, M.L.; González, F.; Muñoz, J.A.; Ballester, A. Reductive leaching of jarosites by *Aeromonas hydrophila*. *Min. Eng.* **2016**, *95*, 21–28. [CrossRef]
26. Han, R.; Liu, T.; Li, F.; Li, X.; Chen, D.; Wu, Y. Dependence of secondary mineral formation on Fe(II) production from ferrihydrite reduction by *Shewanella oneidensis* MR-1. *ACS Earth Space Chem.* **2018**, *2*, 399–409. [CrossRef]
27. Poggenburg, C.; Mikutta, R.; Schippers, A.; Dohrmann, R.; Guggenberger, G. Impact of natural organic matter coatings on the microbial reduction of iron oxides. *Geochim. Cosmochim. Acta* **2018**, *224*, 223–248. [CrossRef]
28. Maitte, B.; Jorand, F.P.A.; Grgic, D.; Abdelmoula, M.; Carteret, C. Remineralization of ferrous carbonate from bioreduction of natural goethite in the Lorraine iron ore (Minette) by *Shewanella putrefaciens*. *Chem. Geol.* **2015**, *412*, 48–58. [CrossRef]
29. Jorand, F.; Zegeye, A.; Ghanbaja, J.; Abdelmoula, M. The formation of green rust induced by tropical river biofilm components. *Sci. Total Environ.* **2011**, *409*, 2586–2596. [CrossRef]
30. Crowe, S.A.; O'Neill, A.H.; Weisener, C.G.; Kulczycki, E.; Fowle, D.A.; Roberts, J.A. Reductive dissolution of trace metals from sediments. *Geomicrobiol. J.* **2007**, *24*, 157–165. [CrossRef]
31. Landa, E.R.; Phillips, E.J.P.; Lovley, D.R. Release of 226Ra from uranium mill tailings by microbial Fe(III) reduction. *Appl. Geochem.* **1991**, *6*, 647–652. [CrossRef]
32. Lovley, D.R.; Stolz, J.F.; Nord, G.L.; Phillips, E.J.P. Anaerobic production of magnetite by a dissimilatory iron-reducing microorganism. *Nature* **1987**, *330*, 252–254. [CrossRef]
33. Fredrickson, J.K.; Zachara, J.M.; Kennedy, D.W.; Dong, H.; Onstott, T.C.; Hinman, N.W.; Li, S.M. Biogenic iron mineralization accompanying the dissimilatory reduction of hydrous ferric oxide by a groundwater bacterium. *Geochim. Cosmochim. Acta* **1998**, *62*, 3239–3257. [CrossRef]
34. Vali, H.; Weiss, B.; Li, Y.-L.; Sears, S.K.; Kim, S.S.; Kirschvink, J.L.; Zhang, C.L. Formation of tabular single-domain magnetite induced by *Geobacter metallireducens* GS-15. *Proc. Nat. Acad. Sci. USA* **2004**, *101*, 16121–16126. [CrossRef] [PubMed]
35. Stapleton, R.D., Jr.; Sabree, Z.L.; Palumbo, A.V.; Moyer, C.L.; Devol, A.H.; Roh, Y.; Zhou, J. Metal reduction at cold temperatures by *Shewanella* isolates from various marine environments. *Aquat. Microb. Ecol.* **2005**, *38*, 81–91. [CrossRef]
36. Byrne, J.M.; Telling, N.D.; Coker, V.S.; Pattrick, R.A.D.; van der Laan, G.; Arenholz, E.; Tuna, F.; Lloyd, J.R. Control of nanoparticle size, reactivity and magnetic properties during the bioproduction of magnetite by *Geobacter sulfurreducens*. *Nanotechnology* **2011**, *22*, 455709. [CrossRef]
37. Perez-Gonzalez, T.; Jimenez-Lopez, C.; Neal, A.L.; Rull-Perez, F.; Rodriguez-Navarro, A.; Fernandez-Vivas, A.; Iañez-Pareja, E. Magnetite biomineralization induced by *Shewanella oneidensis*. *Geochim. Cosmochim. Acta* **2010**, *74*, 967–979. [CrossRef]
38. Perez-Gonzalez, T.; Valverde-Tercedor, C.; Yebra-Rodriguez, A.; Prozorov, T.; Gonzalez-Muñoz, M.T.; Arias-Peñalver, J.M.; Jimenez-Lopez, C. Chemical purity of *Shewanella oneidensis*-induced magnetites. *Geomicrobiol. J.* **2013**, *30*, 731–748. [CrossRef]
39. Klueglein, N.; Lösekann-Behrens, T.; Obst, M.; Behrens, S.; Appel, E.; Kappler, A. Magnetite formation by the novel Fe(III)-reducing *Geothrix fermentans* strain HradG1 isolated from a hydrocarbon-contaminated sediment with increased magnetic susceptibility. *Geomicrobiol. J.* **2013**, *30*, 863–873. [CrossRef]
40. Li, C.; Yi, X.; Dang, Z.; Yu, H.; Zeng, T.; Wei, C.; Feng, C. Fate of Fe and Cd upon microbial reduction of Cd-loaded polyferric flocs by *Shewanella oneidensis* MR-1. *Chemosphere* **2016**, *144*, 2065–2072. [CrossRef] [PubMed]
41. Lin, T.J.; Sebae, G.E.; Jung, J.-H.; Jung, D.-H.; Park, C.-S.; Holden, J.F. *Pyrodictium delaneyi* sp. nov., a hyperthermophilic autotrophic archaeon that reduces Fe(III) oxide and nitrate. *Int. J. Syst. Evol. Microbiol.* **2016**, *66*, 3372–3376. [CrossRef] [PubMed]
42. Markovski, C.; Byrne, J.M.; Lalla, E.; Lozano-Gorrín, A.D.; Klingelhöfer, G.; Rull, F.; Kappler, A.; Hoffmann, T.; Schröder, C. Abiotic versus biotic iron mineral transformation studied by a miniaturized backscattering Mössbauer spectrometer (MIMOS II), X-ray diffraction and Raman spectroscopy. *Icarus* **2017**, *296*, 49–58. [CrossRef]
43. Zachara, J.M.; Kukkadapu, R.K.; Fredrickson, J.K.; Gorby, Y.A.; Smith, S.C. Biomineralization of poorly crystalline Fe(III) oxides by dissimilatory metal reducing bacteria (DMRB). *Geomicrobiol. J.* **2002**, *19*, 179–207. [CrossRef]
44. Parmar, N.; Gorby, Y.A.; Beveridge, T.J.; Ferris, F.G. Formation of green rust and immobilization of nickel in response to bacterial reduction of hydrous ferric oxide. *Geomicrobiol. J.* **2001**, *18*, 375–385. [CrossRef]
45. Revesz, E.; Fortin, D.; Paktunc, D. Reductive dissolution of arsenical ferrihydrite by bacteria. *Appl. Geochem.* **2016**, *66*, 129–139. [CrossRef]
46. Revesz, E.; Fortin, D.; Paktunc, D. Reductive dissolution of scorodite in the presence of *Shewanella* sp. CN32 and *Shewanella* sp. ANA-3. *Appl. Geochem.* **2015**, *63*, 347–356. [CrossRef]
47. Zachara, J.M.; Fredrickson, J.K.; Smith, S.C.; Gassman, P.L. Solubilization of Fe(III) oxide-bound trace metals by a dissimilatory Fe(III) reducing bacterium. *Geochim. Cosmochim. Acta* **2001**, *65*, 75–93. [CrossRef]
48. Ghorbanzadeh, N.; Kumar, R.; Lee, S.H.; Park, H.S.; Jeon, B.H. Impact of *Shewanella oneidensis* on heavy metals remobilization under reductive conditions in soil of Guilan Province, Iran. *Geosci. J.* **2018**, *22*, 423–432. [CrossRef]

49. Yang, Y.; Wang, S.; Albrecht-Schmitt, T.E. Microbial dissolution and reduction of uranyl crystals by *Shewanella oneidensis* MR-1. *Chem. Geol.* **2014**, *387*, 59–65. [CrossRef]
50. Um Ano Do Rompimento de Fundão. Available online: https://www.samarco.com/wp-content/uploads/2020/12/Book-Samarco_final_baixa.pdf (accessed on 2 January 2021).
51. Morgenstern, N.R.; Vick, S.G.; Viotti, C.B.; Watts, B.D. Fundão Tailings Dam Review Panel—Report on the Immediate Causes of the Failure of Fundão Dam. Available online: http://fundaoinvestigation.com/wp-content/uploads/general/PR/en/FinalReport.pdf (accessed on 2 January 2021).
52. Carmo, F.F.; Kamino, L.H.Y.; Tobias Junior, R.; Campos, I.C.; Carmo, F.F.; Silvino, G.; Castro, K.J.S.X.; Mauro, M.L.; Rodrigues, N.U.A.; Miranda, M.P.S.; et al. Fundão tailings dam failures: The environment tragedy of the largest technological disaster of Brazilian mining in global context. *Persp. Ecol. Cons.* **2017**, *15*, 145–151. [CrossRef]
53. Valeriano, C.M.; Neumann, R.; Alkmim, A.R.; Evangelista, H.; Heilbron, M.; Aguiar Neto, C.C.; Souza, G.P. Sm-Nd and Sr isotope fingerprinting of iron mining tailing deposits spilled from the failed SAMARCO Fundão dam 2015 accident at Mariana, SE-Brazil. *Appl. Geochem.* **2019**, *106*, 34–44. [CrossRef]
54. Reis, D.A.; Nascimento, L.P.; Abreu, A.T.; Nalini Június, H.A.; Roeser, H.M.P.; Santiago, A.F. Geochemical evaluation of bottom sediments affected by historic mining and the rupture of the Fundão dam, Brazil. *Environ. Sci. Pol. Res.* **2020**, *27*, 4365–4375. [CrossRef] [PubMed]
55. Schettini, C.A.F.; Hatje, V. The suspended sediment and metals load from the Mariana's tailing dam failure to the coastal sea. *Integr. Environ. Assessm. Manag.* **2020**, *16*, 661–668. [CrossRef]
56. Viana, L.M.S.; Pestana, I.A.; Carvalho, C.E.V.; Salomão, M.S.M.B. Doce River estuary: Geochemical changes following the largest tailing spill in South America. *Arch. Environ. Contam. Toxicol.* **2020**, *79*, 343–353. [CrossRef] [PubMed]
57. Almeida, C.A.; Oliveira, A.F.; Pacheco, A.A.; Lopes, R.P.; Neves, A.A.; Queiroz, M.E.L.R. Characterization and evaluation of sorption potential of the iron mine waste after Samarco dam disaster in Doce River basin—Brazil. *Chemosphere* **2018**, *209*, 411–420. [CrossRef] [PubMed]
58. Queiroz, H.M.; Nóbrega, G.N.; Ferreira, T.O.; Almeida, L.S.; Romero, T.B.; Santaella, S.T.; Bernardino, A.F.; Otero, X.L. The Samarco mine tailing disaster: A possible time-bomb for heavy metals contamination? *Sci. Total Environ.* **2018**, *637–638*, 498–506. [CrossRef] [PubMed]
59. Jardim, F.A.; von Sperling, E.; Jardim, B.F.M.; Almeida, K.C.B. Fatores determinantes das florações de cianobactérias na água do Rio Doce, Minas Gerais, Brasil. *Eng. Sanit. Ambient.* **2014**, *19*, 207–218. [CrossRef]
60. Richard, E.C.; Duarte, H.A., Jr.; Estrada, G.C.D.; Bechtold, J.-P.; Maioli, B.G.; Freitas, A.H.A.; Warner, K.E.; Figueiredo, L.H.M. Influence of Fundão tailings dam breach on water quality in the Doce River watershed. *Integr. Environ. Assessm. Manag.* **2020**, *16*, 585–595. [CrossRef]
61. Wolin, E.A.; Wolin, M.J.; Wolfe, R.S. Formation of methane by bacterial extracts. *J. Biol. Chem.* **1963**, *238*, 2882–2886. [CrossRef]
62. McLaughlin, J.R.; Ryden, J.C.; Skyers, J.K. Sorption of inorganic phosphate by iron- and aluminum-containing components. *Eur. J. Soil Sci.* **1981**, *32*, 365–378. [CrossRef]
63. Viollier, E.; Inglett, P.W.; Hunter, K.; Roychoudhury, A.N.; Van Cappellen, P. The ferrozine method revisited: Fe(II)/Fe(III) determination in natural waters. *Appl. Geochem.* **2000**, *15*, 785–790. [CrossRef]
64. Jurelevicius, D.; Alvarez, V.M.; Marques, J.M.; Lima, L.R.F.S.; Dias, F.A.; Seldin, L. Bacterial community response to petroleum hydrocarbon amendments in freshwater, marine, and hypersaline water-containing microcosms. *Appl. Environ. Microbiol.* **2013**, *79*, 5927–5935. [CrossRef]
65. Pitcher, D.G.; Saunders, N.A.; Owen, R.J. Rapid extraction of bacterial genomic DNA with guanidium thiocyanate. *Let. Appl. Microbiol.* **1989**, *8*, 151–156. [CrossRef]
66. Hammer, O.; Harper, D.A.T.; Ryan, P.D. PAST: Palaeontological statistics software package for education and data analysis. *Palaeontol. Electron.* **2001**, *4*, 1–9.
67. Anderson, M.J. A new method for non-parametric multivariate analysis of variance. *Austral Ecol.* **2001**, *26*, 32–46.
68. Tintelnot, M.; Brichta, A.; Morais, J.O. Clay Mineralogy of River Sediments on the Brazilian Coast. In Proceedings of the Berichte der DTTG e.V.—Band 6, Jahrestagung der DTTG, Greifswald, Germany, 3–5 September 1998; Available online: http://www.dttg.ethz.ch/cd_dttg1998/tintelnot/tintelnot.htm (accessed on 23 December 2020).
69. Sparks, N.H.C.; Mann, S.; Bazylinski, D.A.; Lovley, D.R.; Jannasch, H.W.; Frankel, R.B. Structure and morphology of magnetite anaerobically-produced by a marine magnetotactic bacterium and a dissimilatory iron-reducing bacterium. *Earth Planet. Sci. Let.* **1990**, *98*, 14–22. [CrossRef]
70. Lagroix, F.; Guyodo, Y. A new tool for separating the magnetic mineralogy of complex mineral assemblages from low temperature magnetic behavior. *Front. Earth Sci.* **2017**, *5*, 61. [CrossRef]
71. Dormann, J.L.; Fiorani, D.; Tronc, E. Magnetic relaxation in fine-particle system. *Adv. Chem. Phys.* **1997**, *98*, 283.
72. Guardia, P.; Batlle-Brugal, B.; Roca, A.G.; Iglesias, O.; Morales, M.D.P.; Serna, C.J.; Batlle, X. Surfactant effects in magnetite nanoparticles of controlled size. *J. Magn. Magn. Mater.* **2007**, *316*, e756–e759. [CrossRef]
73. Rondinone, A.J.; Samia, A.C.S.; Zhang, Z.J. Superparamagnetic relaxation and magnetic anisotropy energy distribution in $CoFe_2O_4$ spinel ferrite nanocrystallites. *J. Phys. Chem. B* **1999**, *103*, 6876. [CrossRef]
74. Granitzer, P.; Rumpf, K.; Venkatesan, M.; Roca, A.G.; Cabrera, L.; Morales, M.P.; Poelt, P.; Albu, M. Magnetic study of Fe_3O_4 nanoparticles incorporated within mesoporous silicon. *J. Electrochem. Soc.* **2010**, *157*, K145–K151. [CrossRef]

75. Kodama, R.H.; Berkowitz, A.E.; McNiff, E.J., Jr.; Foner, S. Surface spin disorder in ferrite nanoparticles. *J. Appl. Phys.* **1997**, *81*, 5552–5557. [CrossRef]
76. Muscas, G.; Concas, G.; Cannas, C.; Musinu, A.N.N.A.; Ardu, A.; Orrù, F.; Peddis, D. Magnetic properties of small magnetite nanocrystals. *J. Phys. Chem. C* **2013**, *117*, 23378–23384. [CrossRef]
77. Zysler, R.D.; Fiorani, D.; Testa, A.M. Investigation of magnetic properties of interacting Fe_2O_3 nanoparticles. *J. Magn. Magn. Mater.* **2001**, *224*, 5–11. [CrossRef]
78. Gittleman, J.I.; Abeles, B.; Bozowski, S. Superparamagnetism and relaxation effects in granular Ni-SiO_2 and Ni-Al_2O_3 films. *Phys. Rev. B* **1974**, *9*, 3891. [CrossRef]
79. Nunes, W.C.; Socolovsky, L.M.; Denardin, J.C.; Cebollada, F.; Brandl, A.L.; Knobel, M. Role of magnetic interparticle coupling on the field dependence of the superparamagnetic relaxation time. *Phys. Rev. B* **2005**, *72*, 212413. [CrossRef]
80. Cullity, B.D. *Introduction to Magnetic Materials*; Addison-Wesley: Reading, MA, USA, 1972.
81. Lima, E.; Brandl, A.L.; Arelaro, A.D.; Goya, G.F. Spin disorder and magnetic anisotropy in Fe_3O_4 nanoparticles. *J. Appl. Phys.* **2006**, *99*, 083908. [CrossRef]
82. Mamiya, H.; Fukumoto, H.; Cuya Huaman, J.L.; Suzuki, K.; Miyamura, H.; Balachandran, J. Estimation of magnetic anisotropy of individual magnetite nanoparticles for magnetic hyperthermia. *ACS Nano* **2020**, *14*, 8421–8432. [CrossRef] [PubMed]
83. Stoner, E.C.; Wohlfarth, E.P. A mechanism of magnetic hysteresis in heterogeneous alloys. *IEEE Trans. Magn.* **1991**, *27*, 3475–3518. [CrossRef]
84. Hadjipanayis, G.; Sellmyer, D.J.; Brandt, B. Rare-earth-rich metallic glasses. I. Magnetic hysteresis. *Phys. Rev. B* **1981**, *23*, 3349–3354. [CrossRef]
85. Machala, L.; Zboril, R.; Gedanken, A. Amorphous iron (III) oxide a review. *J. Phys. Chem. B* **2007**, *111*, 4003–4018. [CrossRef]
86. Bell, P.E.; Mills, A.L.; Herman, J.S. Biogeochemical conditions favoring magnetite formation during anaerobic iron reduction. *Appl. Environ. Microbiol.* **1987**, *53*, 2610–2616. [CrossRef] [PubMed]
87. Roh, Y.; Moon, H.-S. Iron reduction by a psychrotolerant Fe(III)-reducing bacterium isolated from ocean sediment. *Geosci. J.* **2001**, *5*, 183–190. [CrossRef]
88. Winklhofer, M.; Petersen, N. Paleomagnetism and magnetic bacteria. In *Magnetoreception and Magnetosomes in Bacteria*; Schüler, D., Ed.; Springer: Berlin/Heidelberg, Germany, 2006; pp. 255–273. [CrossRef]
89. Frankel, R.B. Anaerobes pumping iron. *Nature* **1987**, *330*, 208. [CrossRef]
90. Berny, C.; Le Fèvre, R.; Guyot, F.; Blondeau, K.; Guizonne, C.; Rousseau, E.; Bayan, N.; Alphandéry, E. A method for producing highly pure magnetosomes in large quantity for medical applications using *Magnetospirillum gryphiswaldense* MSR-1 magnetotactic bacteria amplified in minimal growth media. *Front. Bioeng. Biotechnol.* **2020**, *8*, 16. [CrossRef]
91. Ahn, T.; Kim, J.H.; Yang, H.-M.; Lee, J.W.; Kim, J.-D. Formation pathways of magnetite nanoparticles by coprecipitation method. *J. Phys. Chem.* **2012**, *116*, 6069–6076. [CrossRef]
92. Yan, W.; Zhou, J.; Liu, H.; Chen, H.; Zhang, Y.; Wei, Y. Formation of goethite and magnetite rust via reaction with Fe(II). *J. Electrochem. Soc.* **2016**, *163*, C289–C295. [CrossRef]
93. Giongo, A.; Borges, L.G.A.; Marconatto, L.; Palhano, P.L.; Serbent, M.P.; Moreira-Silva, E.; Siqueira, T.A.; Martinho, C.T.; Barili, R.; Paz, L.V.; et al. Adaption of microbial communities to the hostile environment in the Doce River after the collapse of two iron ore tailing dams. *Heliyon* **2020**, *6*, e04778. [CrossRef] [PubMed]
94. Reis, M.P.; Suhadolnik, M.L.S.; Dias, M.F.; Ávila, M.P.; Motta, A.M.; Barbosa, F.A.R.; Nascimento, A.M.A. Characterizing a riverine microbiome impacted by extreme disturbance caused by a mining sludge tsunami. *Chemosphere* **2020**, *253*, 126584. [CrossRef]
95. Postma, D. Formation of siderite and vivianite and the pore-water composition of a recent bog sediment in Denmark. *Chem. Geol.* **1981**, *31*, 225–244. [CrossRef]
96. Aller, R.C.; Mackin, J.E.; Cox, R.T. Diagenesis of Fe and S in Amazon inner shelf muds: Apparent dominance of Fe reduction and implications for the genesis of ironstones. *Cont. Shelf Res.* **1986**, *6*, 263–289. [CrossRef]
97. Karlin, R.; Lyle, M.; Heath, G. Authigenic magnetite formation in suboxic marine sediments. *Nature* **1987**, *326*, 490–493. [CrossRef]
98. Blöthe, M.; Roden, E.E. Microbial iron redox cycling in a circumneutral-pH groundwater seep. *Appl. Environ. Microbiol.* **2009**, *75*, 468–473. [CrossRef] [PubMed]
99. Du Laing, G.; Rinklebe, J.; Vandecasteele, B.; Meers, E.; Tack, F.M.G. Trace metal behaviour in estuarine and riverine floodplain soils and sediments: A review. *Sci. Total Environ.* **2009**, *407*, 3972–3985. [CrossRef]
100. Vuillemin, A.; Friese, A.; Wirth, R.; Schuessler, J.A.; Schleicher, A.M.; Kemnitz, H.; Lücke, A.; Bauer, K.W.; Nomosatryo, S.; von Blanckenburg, F.; et al. Vivianite formation in ferruginous sediments from Lake Towuti, Indonesia. *Biogeosciences* **2020**, *17*, 1955–1973. [CrossRef]
101. Stumm, W.; Sulzberger, B. The cycling of iron in natural environments: Considerations based on laboratory studies of heterogeneous redox processes. *Geochim. Cosmochim. Acta* **1992**, *56*, 3233–3257. [CrossRef]
102. Lynch, S.F.L.; Batty, L.C.; Byrne, P. Environmental risk of metal mining contaminated river bank sediment at redox-transitional zones. *Minerals* **2014**, *4*, 52–73. [CrossRef]
103. Fortin, D.; Leppard, G.G.; Tessier, A. Characteristics of lacustrine diagenetic iron oxyhydroxides. *Geochim. Cosmochim. Acta* **1993**, *57*, 4391–4404. [CrossRef]
104. Melton, E.D.; Swanner, E.D.; Behrens, S.; Schmidt, C.; Kappler, A. The interplay of microbially mediated and abiotic reactions in the biogeochemical Fe cycle. *Nat. Rev. Microbiol.* **2014**, *12*, 797–808. [CrossRef]

105. Emerson, D.; Revsbech, N.P. Investigation of an iron-oxidizing microbial mat community located near Aarhus, Denmark: Field studies. *Appl. Environ. Microbiol.* **1994**, *60*, 4022–4031. [CrossRef]
106. Dekov, V.M.; Vanlierde, E.; Billström, K.; Garbe-Schönberg, C.-D.; Weiss, D.J.; Gatto Rotondo, G.; Van Meel, K.; Kuzmann, E.; Fortin, D.; Darchuk, L.; et al. Ferrihydrite precipitation in groundwater-fed river systems (Nete and Demer river basins, Belgium): Insights from a combined Fe-Zn-Sr-Nd-Pb-isotope study. *Chem. Geol.* **2014**, *386*, 1–15. [CrossRef]
107. Johnston, S.G.; Rose, A.L.; Burton, E.D.; Webster-Brown, J. Landslide-induced iron mobilisation shapes benthic accumulation of nutrients, trace metals and REE fractionation in an oligotrophic alpine stream. *Geochim. Cosmochim. Acta* **2015**, *148*, 1–22. [CrossRef]
108. Posth, N.R.; Canfield, D.E.; Kappler, A. Biogenic Fe(III) minerals: From formation to diagenesis and preservation in the rock record. *Earth-Sci. Rev.* **2014**, *135*, 103–121. [CrossRef]
109. Baken, S.; Salaets, P.; Desmet, N.; Seuntjens, P.; Vanlierde, E.; Smolders, E. Oxidation of iron causes removal of phosphorus and arsenic from streamwater in groundwater-fed lowland catchments. *Environ. Sci. Technol.* **2015**, *49*, 2885–2894. [CrossRef] [PubMed]
110. De Vitri, R.; Belzile, N.; Tessier, A. Speciation and adsorption of arsenic on diagenetic iron oxyhydroxides. *Limnol. Oceanogr.* **1991**, *36*, 1480–1485. [CrossRef]
111. Lienemann, C.-P.; Monnerat, M.; Dominik, J.; Perret, D. Identification of stoichiometric iron-phosphorus colloids produced in a eutrophic lake. *Aquat. Sci.* **1999**, *61*, 133–149. [CrossRef]
112. Gounot, A.M. Microbial oxidation and reduction of manganese: Consequences in groundwater and applications. *FEMS Microbiol. Rev.* **1994**, *14*, 339–350. [CrossRef]
113. Fraga, M.S.; Reis, G.B.; Silva, D.D.; Guedes, H.A.S.; Elesbon, A.A.A. Use of multivariate statistical methods to analyze the monitoring of surface water quality in the Doce River basin, Minas Gerais, Brazil. *Environ. Sci. Pol. Res.* **2020**, *27*, 35303–35318. [CrossRef] [PubMed]